**The regulation of mitotic spindle orientation by BRCA1 controls the proliferation, polarization and growth arrest of human mammary epithelia**

by

Oksana Nemirovsky

B.Sc., The University of Victoria, 2009

A THESIS SUBMITED IN PARTIAL FULFILLMENT OF

THE REQUIRMENTS FOR THE DEGREE OF

MASTER OF SCIENCE

in

The Faculty of Graduate and Postdoctoral Studies

(Experimental Medicine)

THE UNIVERSITY OF BRITISH COLUMBIA

(VANCOUVER)

AUGUST 2014

**Abstract**

Carriers of mutations in the *Breast Cancer 1* (*BRCA1)* gene have an increased risk to develop breast cancer, which tend to be early-onset, lack expression of estrogen receptor, progesterone receptor and human epidermal growth factor receptor 2, and resemble basal epithelia by gene expression. The phenotypic resemblance of these tumours to normal stem/progenitor cells suggests that the loss of BRCA1 function may dysregulate stem cell maintenance and differentiation. In model organisms, a mechanism that promotes the generation of daughter cells different from a mother stem cell is the asymmetric segregation of non-genetic factors through mitotic spindle orientation. BRCA1 regulates mitotic spindle assembly through the post-transcriptional degradation of the low-penetrance breast cancer susceptibility gene product RHAMM and the abundance of RHAMM influences mitotic spindle orientation by regulating its movement along the cell cortex.

This led to the hypothesis that BRCA1 is necessary for the correct orientation of the mitotic spindle in mammary epithelial cells, which controls their proliferation, polarization and growth arrest. To address this hypothesis, I studied non-malignant human mammary cell-lines and primary human progenitor cell-enriched populations. BRCA1 was silenced by shRNA introduced through lentiviral transduction. Silencing of BRCA1 in cell-lines increased both mitotic and post-mitotic abnormalities, including the loss of spindle orientation with subsequent lagging chromosomes and micronucleus formation in 2D cultures. The consequence of these defects included a significant decrease in colony-forming capacity.

I then enquired whether BRCA1 is necessary for MCF10A cells to proliferate, form polarized acini, and growth arrest in 3D cultures. Control cells underwent planar division to form polarized, growth arrested acini, while BRCA1 silenced structures were larger, less polarized and more proliferative. Loss of correct spindle orientation was also observed.

These results indicate that BRCA1 plays a role in maintaining the integrity of human mammary cell division. Loss of BRCA1 induces mitotic and post-mitotic consequences that impair cellular proliferative capacity and abolish ability to undergo directional division, polarization and arrest growth. These findings thus raise the possibility that breast cancer treatments aimed at counteracting the BRCA1-mediated loss of polarity may complement drugs that combat the diminished DNA repair characteristic of BRCA1-associated tumours.

## Preface

Collaborators from Germany provided the following doxycycline inducible mammary cell-lines: non-malignant, estrogen responsive MCF12A cells (MCF12A native), MCF12A expressing scrambled shRNA (MCF12A shScr), and MCF12A expressing shRNA targeting BRCA1 (MCF12A shBRCA1).

The work I present in chapter 3.6 was done in collaboration with Dr. N Kannan, a post-doctoral fellow in the laboratory of Dr. CJ Eaves (BC Cancer Research Center, Terry Fox Labs). Dr. N Kannan used fluorescence activated cell sorting to isolate highly enriched populations of luminal progenitors and basal cells from human normal reduction mammoplasty samples. Dr. Kannan cultured these cells in reconstituted basement membrane (Matrigel) cultures as previously described.[1] I performed the immunostaining and further analysis of the resultant acinar structures.

The Western blot analysis of BRCA1 expression levels in MCF12A cells was performed by Helen Chen and Pooja Mohan (Dr. CA Maxwell lab, Child and Family Research Institute).

**Table of Contents**

**List of Tables**

**List of Figures**

**List of Abbreviations**

| | |
|---|---|
| AKI | Aurora Kinase A Inhibitor |
| ATM | Ataxia telangiectasia |
| AURKA | Aurora Kinase A |
| BC | Basal Cells |
| BP | Basal Progenitors |
| BRCA1 | Breast Cancer 1, early onset |
| BRCA2 | Breast Cancer 2, early onset |
| BSA | Bovine Serum Albumin |
| CD49f | Integrin |
| CFC | Colony forming cell |
| DAPI | 4’,6-diamidino-2-phenylindol |
| DMEM | Dulbecco’s Modified Eagle Medium |
| DMSO | Dimethyl Sulfoxide |
| DNA | Deoxyribonucleic acid |
| Dox | Doxycycline |
| EGF | Epidermal Growth Factor |
| EpCAM | Epithelial adhesion molecule |
| ER | Estrogen receptor |
| FA | Fanconi Anemia |
| FACS | Fluorescence-Activated Cell Sorting |
| FBS | Fetal Bovine Serum |
| GEP | Gene expression profiling |

| | |
|---|---|
| GFP | Green fluorescent protein |
| HER-2 | Human epidermal growth factor receptor |
| *HMMR* | Hyaluronan Mediated Motility Receptor |
| IF | Immunofluorescence |
| iPS | Induced pluripotent stem cells |
| LP | Luminal progenitors |
| mESC | Mouse Embryonic Stem Cells |
| MM | Master Mix |
| NHP | non-hairpin |
| NuMA | Nuclear mitotic apparatus protein |
| PBS | Phosphate Buffered Saline |
| PFA | Paraformaldehyde |
| PLK1 | Polo-like kinase 1 |
| PLK2 | Polo-like kinase 2 |
| rBM | Reconstituted basement membrane (Matrigel) |
| RFP | Red fluorescent protein |
| RHAMM | Receptor for Hyaluronan Mediated Motility |
| RNA | Ribonucleic acid |
| SC | Stromal cells |
| SCR | shRNA scrambled control |
| SDS | Sodium dodecyl sulfate |
| SEM | Standard error of the mean |
| shRNA | Small hairpin RNA |

| | |
|---|---|
| sh1BRCA1 | sh34BRCA1 shRNA |
| sh2BRCA1 | sh37BRCA1 shRNA |
| SNP | Single Nucleotide Polymorphism |
| TNP | Triple negative phenotype |
| TPX2 | Targeting protein for Xklp2 |
| TubB | Tubulin B |
| TubG1 | Gamma-tubulin 1 |
| WB | Western blot |
| UT | Untreated |
| 2D | Two dimensional |
| 3D | Three dimensional |

**Acknowledgements**

I would like to extend my gratitude to all the women who participated in this study as tissue donors and as study support. I hope my work will benefit you and your families.

Many thanks to all the members of the Maxwell lab, who supported me through this journey.

Thank you Connie, Pauline, James, Alex, Raj and Chris for all the support, great suggestions and wonderful discussions!

**Dedication**

Dedicated to all the women, and the men who supported them.

Галине, Дарье, Вере, Анатолию, Михаилу, Алексею.

# Chapter 1: Introduction

## 1.1 Mammary biology and stem/progenitor cells

Although the development and maintenance of the mammary gland has been well studied, the identification of mammary stem cells was elusive until recently. The identification, isolation and characterization of mammary stem and progenitor cells in both mouse [2, 3] and human mammary tissue [4, 5] were landmark discoveries that have enabled new fields of research in stem cell biology.

### 1.1.1 Normal human mammary biology

After the full development of the gland during puberty, mammary tissue undergoes cycles of expansion and recession throughout the female lifetime, which finally subside with the onset of menopause. Ductal and lobular expansion occurs during each menstrual cycle and throughout pregnancy [6, 7], and are tightly regulated by estrogen and progesterone. This pattern of continuously fluctuating tissue development supports the idea of the presence of primitive cells in the breast that are able to produce the timely expansion of several cell types.

### 1.1.2 Ducts and alveoli are comprised of polarized mammary epithelia

Two continuously linked but structurally distinct components of the bilayered mammary gland - ducts and alveoli - are comprised of two types of epithelial cells. Both of these structures contain apical-basal polarized cuboidal luminal cells that line a centralized lumen and are surrounded by elongated myoepithelial cells adjacent to an outer basement

membrane. These epithelial cells are also surrounded by stromal, adipose and hematopoietic cells. When luminal cells produce milk, the myoepithelial cells contract to push the milk through the ducts and out to the nipple (Figure 1). Cellular polarity is key to the 3-dimensional (3D) structural organization of the mammary gland [8] and to its principal milk producing function.[2, 9]

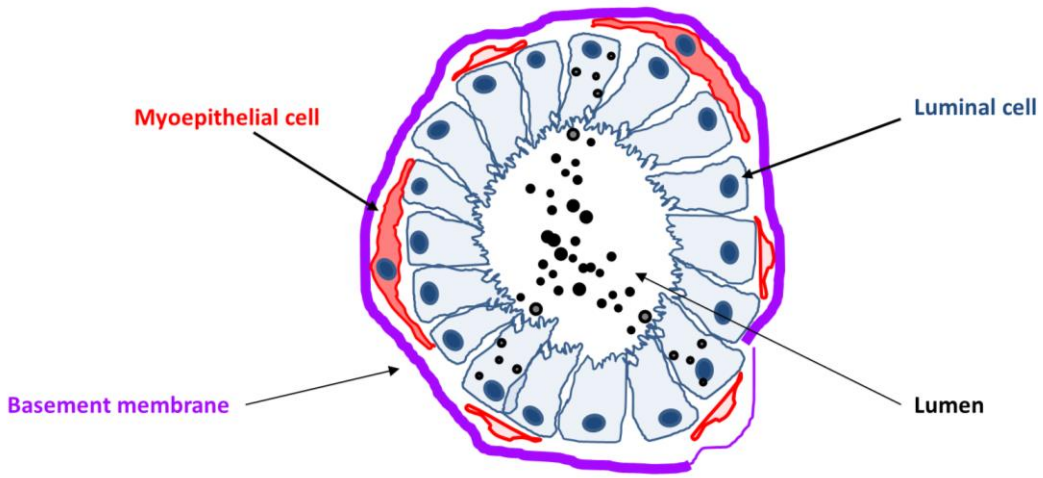


**Figure 1. Cross-section of a normal breast duct.** The lumen is lined with luminal cells, surrounded by a layer of myoepithelial cells. The whole structure is surrounded by a supportive layer of basement membrane. Figure was adapted from Bissell et al 2003.[10]

To establish and maintain correct tissue architecture, cells in the mammary gland polarize organelles and proteins, which is vital for cellular signaling and subsequent behavior.[8] When grown in a 3D context, mammary cells establish apicobasal polarity and undergo planar, polarized cell division; each of these phenotypes plays an important role in the physiological and metabolic functions of these cells.

Apico-basal polarity is important for metabolic functions, such as absorption and secretion of nutrients, proteins (milk), and other molecules, and pathways that establish this polarity contribute to proper tissue architecture. For example, integrin signaling is necessary

to establish polarity in mammary 3D spheroids and, upon destruction of integrin signaling, polarization is not observed and lumens are not formed.[11] Furthermore, apicobasal polarity is necessary for normal mammary cell proliferation, as indicated by the finding that the silencing of BRCA1 in MCF10A cells disrupts apico-basal polarity and correlates with an increased size (proliferation) and decreased circularity of cellular structures.[12, 13]

Planar polarity, the polarity exhibited by the adjacent cells relative to each other in one dimension [14], is important for cell to cell and cell to niche signaling during cellular communication and transport. Mitotic polarity, which is instrumental in determining the fate of daughter cells during a stem cell division, is another type of polarity that may enable the asymmetric positioning of the nucleus.[15] Polarity may be disturbed during mammary carcinogenesis. For example, mitotic polarity is lost upon the targeted disruption of p53, but restored upon its activation with an Mdm2 inhibitor.[16]

### 1.1.3 Stem cell hierarchy in human mammary gland

The pattern of continuous mammary development through adult life supports the idea of a hierarchical distribution of cells with varying regenerative and differentiation potential in the breast. An adult human mammary gland contains a rare population of stem cells that generate mammary progenitors, which are in turn responsible for generating terminally differentiated luminal and myoepithelial cell lineages. Cells isolated from the human mammary gland and enriched according to their relative expression of epithelial adhesion marker $(EpCAM)^{low}$ and integrin $(CD49f)^{high}$ have an enhanced in vivo potential to regenerate a mammary gland with luminal and myoepithelial lineages (Figure 2).[4, 5, 9]

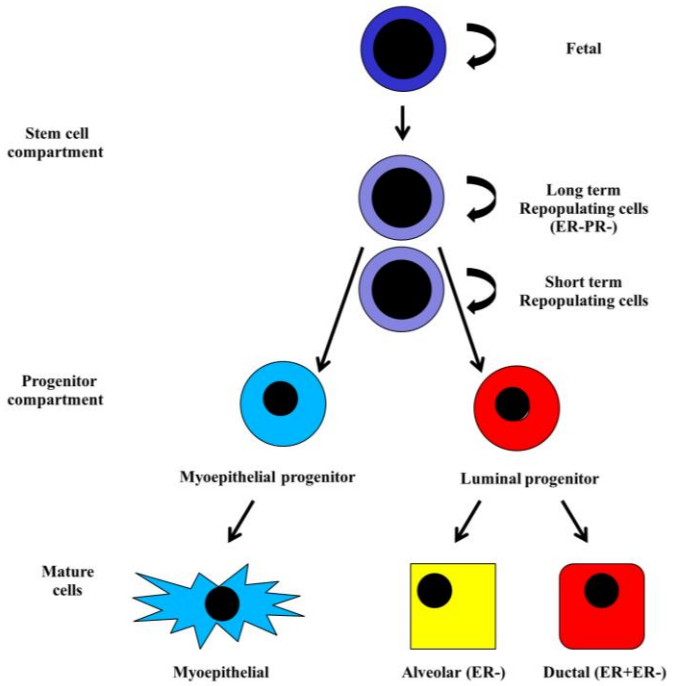


**Figure 2. Mammary stem cell hierarchy.** Mammary stem cells comprise a heterogeneous compartment of mammary epithelia. These cells have capacity to self-renew and differentiate, producing the entire mammary gland. Figure was adapted from Visvader and Stingl, *Genes and Development*, 2014.[17]

### 1.1.4 Controversies surrounding the properties and hierarchy of mammary stem cells

The concept of a stem cell hierarchy posits a certain degree of directionality (i.e. pluripotent stem cells giving rise to terminally differentiated progeny), which, as a fundamental concept, has recently been challenged by a series of studies. Induced pluripotent stem cells (iPS cells) were first described in 2006 when Yamanaka and colleagues forced differentiated fibroblasts to express 4 transcription factors (Oct3/4, Sox2, c-Myc, and Klf4) that caused them to reactivate a stem cell state.[18]

High levels of heterogeneity in the mammary luminal compartment have been described, including the description of cells with variable proliferation and differentiation capacities.[19] Furthermore, some apparently unipotent mammary cells were found to display

high proliferative potential, implying that they also have stem cell activity.[20] Finally, DNA barcoding of mammary cells revealed the presence of cells that generate latent clones that only become apparent in secondary transplants, supporting the idea of plasticity in the proliferative behavior of certain types of mammary gland cells.[21] These studies challenge the concept of a mammary stem cell hierarchy, and raise the possibility of plasticity through which, under the proper conditions and at the right timing [22], any mammary cell could act as a primitive cell with the potential to recapitulate the entire mammary gland.

### 1.1.5 Isolation, quantification and maintenance of primitive mammary cells

While the precise nature and characteristics of mammary stem cells are not fully known, methods have been established to isolate, quantify and maintain primitive mammary fractions that have an increased potential to reconstitute a mammary gland. Fractions that are enriched for mammary stem/progenitor cells can be isolated by fluorescence activated cell sorting (FACS) using specific extracellular cell surface markers.[4, 5, 1] Mammary single cell suspension is pre-depleted of endothelial and hematopoietic cells and isolated based on the expression levels of EPCAM and CD49f to give 3 mammary epithelial populations and stroma: luminal cells (LC), luminal progenitors (LP), basal cells (BC) and stromal cells (SC).[1] The mammary progenitor fractions obtained can be maintained and manipulated in a 3D tissue culture system using reconstituted basement membrane (rBM), also known as matrigel. Matrigel is isolated from Englebreth-Holm-Swarm mouse sarcoma tumours [23] and is comprised primarily of laminin and collagen, although other proteins are present at various concentrations. Thus, lot to lot variation is a concern. However, matrigel cultures support mammary tissue morphogenesis and the propagation and maintenance of mammary

epithelial populations, which could be explained in part by the interaction fostered between CD49f integrins expressed on mammary cells and laminins in matrigel.[1, 24, 7,] Thus, matrigel cultures represent an important tool for the propagation, maintenance, and characterization of non-malignant and/or primary mammary cells.

### 1.2 Classification and predisposition to breast cancer

Breast cancer is a heterogeneous malignancy and individual patients present with unique tumours that have different clinico-pathological histories, progression patterns, and outcomes. In general, breast cancers can be classified based on their size, cellular/tissue morphology, the presence or absence of mutations in key genes, and the expression of various gene products. Furthermore, breast cancers can be classified according to those that occur sporadically (by acquisition of somatic changes) or in a recognized hereditary manner due to the presence of predisposing mutations passed through a family. My research is focused on understanding the mechanisms associated with hereditary breast cancers linked to mutations in *BRCA1*. These breast tumours tend to be classified as basal-like by their gene expression profiles and triple negative (for a lack of expression of estrogen, progesterone and HER2 receptors) by immunohistochemistry.

#### 1.2.1 Breast cancer subtypes

In a landmark paper, microarray-based gene expression profiling was used to identify five major breast cancer molecular subtypes: luminal A, luminal B, normal-like, Her2 positive and basal-like.[25, 26] These subtypes vary in pathological manifestation, immunohistochemical features, clinical outcomes [26], inferred cells of origin [9, 27], content of

proliferating cells [28], differentiation features [29], preferred sites for metastasis, and disease aggressiveness.[30, 31] The heterogeneity within and between these subtypes suggests that treatment protocols should be more specifically designed to fit the type of the breast cancer. Currently, this poses a problem as targeted treatments are lacking for some sub-types of breast cancers, while others are ineffective due to drug resistance. Therefore, a better understanding of the molecular mechanisms involved in tumourigenesis is needed to combat these heterogeneous diseases and to improve treatment and survival rates for breast cancer.

Luminal A breast cancers are low grade, well differentiated tumours that contain cells that are estrogen receptor (ER) positive; whereas, Luminal B tumours, which are also ER-positive, are higher grade, poorly differentiated tumours.[26] Normal like breast cancers are characterized by a transcript profile that more closely resembles the normal mammary stem cell expression profile.[31, 17] HER2 positive breast cancers are characterized by an elevated expression of epidermal growth factor receptor 2 (erb, HER2 or Neu), which normally controls mammary epithelial cell proliferation and differentiation. HER2 overexpression correlates with breast tumour size, aneuploidy, grade and mitotic status, and infiltration of lymph nodes.[32] Fortunately, trastuzumab (Herceptin), a humanized monoclonal antibody raised against the HER2 extracellular domain, is available as a molecular-targeted therapy for this aggressive subtype of breast cancer.

Basal-like subtype mammary tumours are defined by a gene expression profile that resembles that of normal basal mammary cells. These tumours tend to express what is termed a triple negative phenotype (TNP). That is, these tumours do not express ER, progesterone receptor, and HER2. Basal-like tumours are mostly high grade, poorly differentiated tumours, often appearing in a younger age group.[33] The clinical outcome for

these tumours is particularly poor as the tumours tend to be highly proliferative, aggressive, and metastatic. Moreover, no targeted treatments are available for TNP tumours, as these ER-negative tumours tend to be refractory to anti-estrogens, aromatase inhibitors and Herceptin. Immunopanels consisting of various combinations of markers have been used in an attempt to improve the outcome and find a better prognostic tool for this disease.[34]

### 1.2.2 Inherited mutations that predispose to breast cancer

Sporadic breast cancers account for about 90% of cases and likely occur at random through the interactions between an individual's genetic make-up and exposure to environmental factors. The remaining 10% of cases are hereditary breast cancers, which occur due to known mutations in specific breast cancer predisposition genes.[35] Some of the better documented gene products whose mutations predispose to breast cancer are: Ataxia telangiectasia mutated (*ATM*) [36, 37], Breast cancer 1, early onset (*BRCA1*), Breast cancer 2, early onset (*BRCA2*) [38], and Fanconi Anemia members (*FA*).[39, 40] Importantly, each of these gene products plays an important role in DNA damage repair- most notably within homologous recombination pathways.[37, 41, 42, 43, 44] In addition, mutations in any of these gene products are strongly linked with abnormalities in cell cycle progression, which is most commonly attributed to be a consequence of aberrant DNA damage repair. While mutations in these genes may disrupt common DNA repair pathways, carriers of mutations in *BRCA1* are predisposed to develop basal-like subtype, TNP breast cancers, which distinguish these carriers from those with mutations in *BRCA2* or *FA* genes, who tend to develop Luminal B breast tumours. Disruption of p53, however, appears to be consistent across all breast cancer subtypes.[45]

The gene encoding the receptor for hyaluronan-mediated motility (*HMMR)* is also now known to be a breast cancer susceptibility gene, and variation in the gene associates with an increased breast cancer risk in Ashkenazi Jewish populations [38] and carriers of *BRCA1* mutations.[13] Using CGH-targeted linkage analysis, Nathanson et al identified a genetic locus on chromosome 5q33-35.1, containing the gene that encodes for RHAMM, as a region that modifies breast cancer risk in *BRCA1* mutation carriers.[46] Genomic deletions in 5q region have been found in basal-like subtype breast tumours.[47, 48] while network modeling analysis identified RHAMM as the most biologically connected gene to BRCA1.[38]

### 1.2.3 BRCA1 and BRCA2: shared and unique molecular pathways

BRCA1 is a 220 kDa protein with two functional domains: a RING domain at the amino-terminus and BRCT domains at the carboxy-terminus. The RING domain in BRCA1 complexes with BARD1 to form an active heterodimer with ubiquitin ligase activity, which targets proteins for degradation. For example, RHAMM, a mitotic spindle protein, has been shown to be ubiquitinated by the BRCA1-BARD1 heterodimer [49] as has the mitotic spindle pole component gamma-tubulin (TUBG1).[50] The carboxy terminal BRCT domains interact with various proteins and have been shown to be vital for BRCA1 DNA damage repair function. A detailed review of the roles for BRCA1 and BRCA2 in the DNA damage response is beyond the scope of this thesis (reviewed in [51, 52]) however, it is clear that both gene products interact with each other to target Rad51 at the site of DNA damage and enable repair.[43, 53, 54, 55] No homology exists between the *BRCA1* and *BRCA2* genes.[56]

Mutations in *BRCA1* account for about 30% of hereditary breast cancers.[47] Carriers of mutations in *BRCA1* have an increased risk of developing breast cancer in early adulthood.[57, 58] Some ethnicities are especially prone to this disease, explained by the fact

that they carry a founder mutation in *BRCA1*. These are common in Slavic and Jewish populations of Eastern Europe due to their historical segregation.[59]

Since the discovery of the association between mutations in *BRCA1* and early onset breast cancer [60, 44], over 3500 mutations have now been identified in *BRCA1* and are listed in the ClinVar database on PubMed. These mutations span the entire coding region of BRCA1 but certain areas, such as the N-terminal RING domain, exons 11-13, and the BRCT domains, are mutated with a greater frequency [61] (Figure 3). For example, three founder mutations have been identified in Ashkenazi Jewish populations, with 2 of these mutations lying in the N-terminal RING domain (185delAG and 188del11) and one falling in the BRCT domains (5382insC). The N-terminal RING domain in BRCA1 is also the site for heterodimerization with BARD1 and together the BRCA1-BARD1 heterodimer has E3 ubiquitin ligase activity, [62, 63] which is regulated through phosphorylation by aurora kinase A at Ser308.[50, 64] The importance of loss of function in the RING domain to breast cancer tumorigenesis is still unclear. For example, there are striking similarities between the phenotypes of Bard1-null, Brca1-null, and double Bard1;Brca1 null mice (i.e., embryonic lethality, impairment of proliferation, p53 dependence, aneuploidy etc), which suggests convergence of the gene products during development.[65] Moreover, conditional Bard1 null and Brca1 null mice develop breast cancers that are indistinguishable from each other with respect to their frequency, latency, cytogenetics and histology, including expressing basal cytokeratins and lacking receptors for estrogen, progesterone and human epidermal growth factor receptor 2.[66] However, genetically engineered mice expressing inactivated variants of BRCA1 suggest that the E3 ligase activity of BRCA1 may not be essential for mammalian cell viability, HR repair of DNA, or tumor suppression.[67, 68] Thus, the contribution of the N-

terminal RING domain, and the E3 ubiquitin ligase activity, to the tumor suppressive action of BRCA1 is not yet clear.

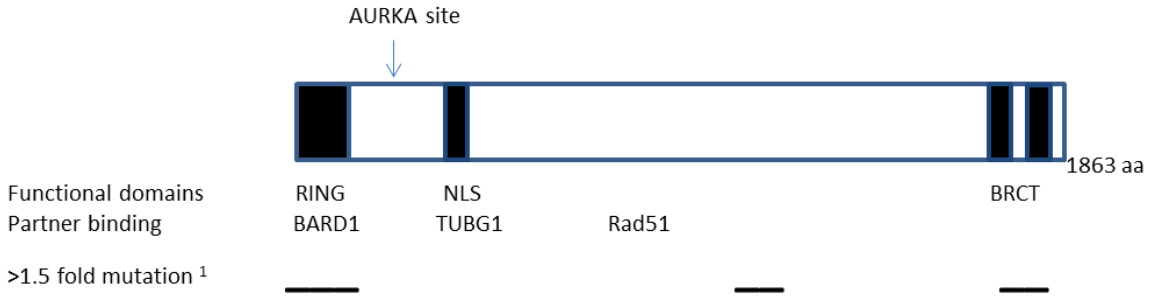


**Figure 3. Simplified schematic for the functional domains in BRCA1, including protein binding partners, and areas in the gene product that are most frequently mutated.** Lines are a schematic representation of the areas with >1.5 fold increase in mutations, as published by Clark et al.[61]

BRCA1 and BRCA2 participate in a shared DNA damage response pathway. However, mutations in these genes predispose carriers to breast tumours with distinct molecular phenotypes.[26, 31] BRCA1-tumours have a very specific pathophysiology: a younger age of occurrence (before 60 years of age), a specific genetic background, and aggressiveness. By gene expression profiling, hereditary BRCA1-mutant tumours differ from sporadic cancers and are usually basal-like subtype.[26, 33, 47] BRCA1- mutant tumours may exhibit a "stem-cell like phenotype" as they are not well differentiated [47] and have therefore been postulated to arise from more primitive mammary cell types.[69, 12, 9] Furthermore, these aggressive, highly mitotic tumours [70] lack targeted therapies [56] and, as a result, have a poor prognosis and reduced survival.[34] The unique pathology of breast tumours in *BRCA1* mutation carriers may indicate the loss of a tumour suppressor pathway that is distinct from the DNA damage response, which should be commonly disrupted with

mutations in *BRCA1, BRCA2,* or *FA* genes. A better understanding of this putative unique tumour suppressor pathway may lead to new therapeutic options for the prevention or treatment of BRCA1-mutant tumours.

### 1.2.4 BRCA1 and the proliferation or differentiation of mammary stem cells

Foulkes first speculated that the pathology and characteristics of BRCA1-mutant tumours may indicate a role for BRCA1 in the regulation of mammary stem cells.[71] Studies using the non-malignant, immortalized MCF10A breast cells demonstrated that the silencing of *BRCA1* was sufficient to disrupt the differentiation and augment the proliferation of these cells in matrigel cultures [12]; in common with the mammary stem/progenitor fraction, MCF10A cells are ER-negative and basal-like by gene expression, and are capable of transiting from a basal-like phenotype to an epithelial (luminal) phenotype during adherent culture.[72, 73, 74] Recent studies in mammary tissues from humans and animals indicate that BRCA1 might control the fate of primitive mammary populations (reviewed in [17]). Briefly, flow cytometric examination of premalignant human breast tissue from *BRCA1* mutation carriers indicated the presence of an expanded luminal progenitor population as compared to breast tissue from normal individuals.[9] These data supported the idea that germline disruption of *BRCA1* may cause expansion of the luminal compartment prior to overt tumourigenesis predisposing this compartment to the subsequent generation of basal-like tumours.[9] This observation was somewhat contradictory to those from Liu et al who previously demonstrated that the complete silencing of BRCA1 within an enriched mammary stem cell population led to a decrease in cells expressing luminal markers and ER, which suggested that BRCA1 was critical to mammary stem cell maintenance.[75]

However, the bulk of recent evidence suggests that the stem cell compartment becomes skewed towards the accumulation of luminal progenitors in carriers of *BRCA1* mutations. Proia and colleagues showed that luminal cells gave rise to tumours in *BRCA1* mutated tissues [27] while Molyneux and colleagues used Blg-Cre $Brca1^{f/f}$ $p53^{+/-}$ mice to specifically disrupt BRCA1 in the luminal compartment and found that the resultant tumours phenocopied human BRCA1-mutant tumours.[69] Furthermore, gene expression profiles of these tumours have established a close association with luminal Sca1-negative, ER-negative cells. Thus, the authors concluded that human BRCA1-mutant tumours are derived from luminal progenitors and not basal progenitors, as previously proposed.[69] Therefore, while the cell-of-origin is not absolutely clear, it is increasingly recognized that BRCA1 plays an important, if not yet completely understood, role in the proliferation and differentiation programs of mammary stem and progenitor cells.[76]

### 1.3 The role of cell division, and mitotic spindle orientation, in stem cell fate

Vidal and colleagues utilized a systems-level analysis to identify novel tumour suppressor pathways that are dysregulated with the loss of BRCA1 function.[38] This analysis identified mitotic spindle assembly gene products (i.e., Aurora kinase A and RHAMM) as putative regulators of tumourigenesis in carriers of *BRCA1* mutations.[38] Before I discuss in detail the mechanistic roles of BRCA1 during cell division, I will first introduce the concept of asymmetric cell division and its potential relevance to balancing expansion and differentiation in a variety of tissue-specific stem cell compartments, including the mammary gland.

### 1.3.1 Symmetric and asymmetric stem cell divisions

Mitosis can be sub-divided into distinct stages (i.e., prophase, prometaphase, metaphase, anaphase, and telophase) based upon the compaction of the DNA and the formation and positioning of a microtubule based mitotic spindle apparatus.[77, 78] Prophase starts the mitotic cycle with the condensation of the chromosomes and migration of the centrosomes (microtubule organizing centers) to the opposite poles of the dividing cell, which then initiates mitotic spindle formation and disruption of the nuclear envelope. During pro-metaphase, the nuclear envelope breaks down to release the condensed chromosomes, which are then captured by microtubules emanating from the duplicated centrosomes to form a bipolar spindle. Metaphase is defined by the equal alignment of the chromosomes at the metaphase plane and the end of metaphase is reliant upon the completion of the spindle assembly checkpoint, which is a biochemical signaling pathway that occurs at each kinetochore to ensure proper chromatid attachment and equal segregation of DNA to the two future daughter cells. Mitotic spindle oscillations occur during metaphase as motor proteins (e.g., dynein) try to locate, capture and tie the mitotic spindle poles to the cortex of the cell in preparation to pull the spindle apart during anaphase.[79] During anaphase, the chromosomes start to move apart to opposite poles of the cell. A functioning spindle assembly checkpoint and correct spindle orientation prevents the unequal distribution of DNA between daughter cells, which is termed aneuploidy and is visible by lagging chromosomes during anaphase. At telophase, a nuclear envelope reforms to enclose each nucleus and a cleavage furrow separates the daughter cells. At the end of telophase, the cleavage furrow disappears, and the daughter cells completely separate.[77, 78] Errors at each step prior to telophase can result in mitotic failure, which can lead to one

daughter cell with a 4N complement of DNA (tetraploidy). Experimentally, mitotic integrity and post-mitotic consequences can be followed precisely by counterstaing the DNA and tubulin staining in both live and fixed cells.

### 1.3.2 Symmetric stem cell divisions

Symmetric divisions of stem cells may produce two daughter cells that both retain stem cell properties (Figure 4). This mode of division expands the pool of stem cells and is important in the context of normal development and responses to tissue injury. The mouse intestinal crypt is first established by symmetric division of stem cells; once the stem cell pool has been established, however, the mode of stem cell division switches to asymmetric division, which maintains the stem cell pool with each division resulting in one daughter stem cell and one daughter differentiated cell [80]. It has been proposed that symmetric divisions may occur at a higher frequency in cancer development, due to mutations or epigenetic changes that dysregulate this process. Alternatively, a stem cell may generate two daughter cells that are both differentiated due to mechanisms that extinguish stem cell properties in both cells. This is referred to as a symmetric differentiation division.

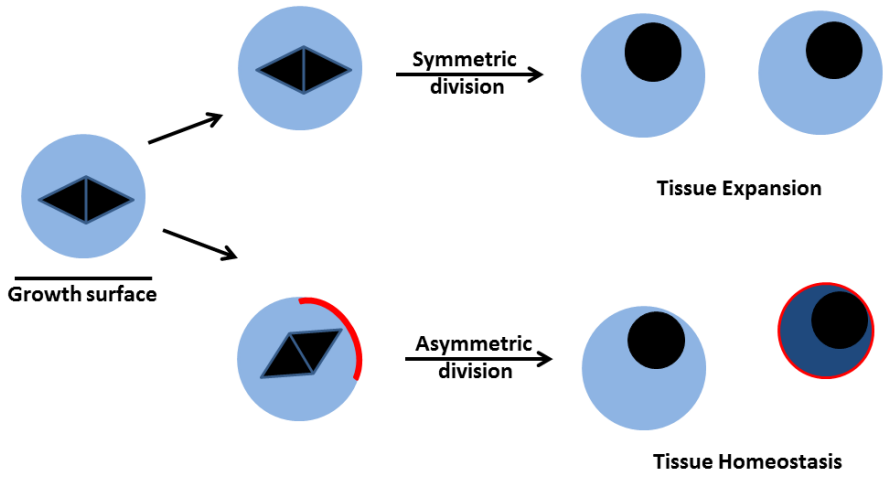


**Figure 4. Symmetric and asymmetric cell division.** Stem cell division may result in asymmetric distribution of fate determinants (shown in red) through mitotic spindle positioning. Even though the progeny are genetically identical, the two cells differ in size and differentiation status.

### 1.3.3 Asymmetric stem cell divisions

Asymmetric division of stem cells refers to a process in which one daughter cell retains stem cell properties and the other one does not (Figure 4). Asymmetric divisions support tissue homeostasis by maintaining the pool of stem cells while also giving rise to progenitor cells that can produce the differentiated cells needed in a given tissue. Upon completion of an asymmetric division, two genetically identical daughter cells are produced with obvious asymmetries in the distribution of some cellular components: mRNA, proteins, and transcription factors.

Examples of such asymmetric divisions and their control have been well described in *Drosophila* neural tissue.[81] In the neuroblast, an asymmetric division results in two daughter cells of differing sizes (a large neuroblast and a small ganglion mother cell) and fates. The fates of the respective daughter cells are largely determined by the asymmetric distribution of fate determining proteins, such as Numb, Miranda and Prospero, within the two daughter

cells, with one of the daughter cells fated to differentiate as a result of selective receipt of transcription factors that drive a differentiation program. Asymmetric cell divisions resulting in the differential distribution of these "fate-determining" elements have also been detected in several mammalian tissues, including hematopoietic [82, 83], skin [84], colon [85], and the mammary gland cells (see also Section 1.3.5). An additional mechanism that may contribute to the repertoire of asymmetries in division progeny is that DNA itself could be asymmetrically segregated. That is, the nonrandom segregation of the Watson and Crick sister chromatids was reported to occur in mouse intestinal tissue.[86]

### 1.3.4 Extrinsic factors that control asymmetric stem cell divisions: intestinal niche

The niche of cells and extracellular molecules that surround a stem cell is thought to play an important role in regulating stem cell behaviour and viability. The mouse intestinal niche is one of the best described in the literature. Intestinal stem cells are localized in the bottom of the crypt in a niche consisting of Paneth and stromal cells. This environment supports a crosstalk between fibroblasts, Paneth cells and $LGR5^+$ intestinal stem cells.[87] Wnt signaling has been implicated in normal crypt maintenance and the support of self-renewal and stemness programs. Wnt signaling is strongest at the bottom of the crypt, and becomes progressively attenuated in cells moving up the crypt.[88] Paneth cells have been shown to control the concentration of Wnt ligands in the crypt and relay these signals to the stem cells.[89] However, to date no evidence of a physically defined stem cell supporting niche has been described in the mammary gland.

Given the importance of local signals and controlled topography in the regulation of many stem cells, it is not surprising that the plane of stem cell division, which is dictated

by the orientation of the mitotic spindle in the dividing cell, has been found to be a principal determinant of asymmetric cell divisions. Thus, in a *Drosophila* neuroblast, a symmetric cell division occurs planar to the niche and results in both daughter stem cells maintaining contact with the niche, and receiving the signals that are critical to the maintenance of "stemness". An asymmetric stem cell division, however, occurs when cells divide perpendicular to the niche, resulting in the release of one daughter cell from the niche to then become a ganglion mother cell that, in turn, gives rise to differentiated neurons and glia cells.

### 1.3.5 Intrinsic factors that control asymmetric stem cell divisions: transcription factors and factors that control mitotic spindle orientation

Asymmetric distribution of transcription factors between two daughter cells can play a critical role in the activation (or not) of differentiation.[81] Mitotic spindle orientation is instrumental to cellular architecture and tissue composition by determining cell fates.[81, 90] The importance of correct mitotic spindle orientation to the differentiation versus self-renewal outcomes of dividing stem cells has been described in a variety of systems, including: *Drosophila* neuroblasts [91], mouse satellite cells [92], human intestinal cells [80], and mouse mammary cells.[93] Moreover, incorrect mitotic spindle positioning has been implicated in neurological diseases and cancer.[94] Thus, spindle orientation together with polarization is likely to be important for proper physiological functioning of tissue-specific stem cells and the prevention of pre-cancerous phenotypes in intestinal [85] and mammary epithelial tissues.[16]

### 1.3.6 Aurora kinase A and Polo-like kinases

Mitosis is a critical process in the development of multicellular organisms and, as such, is under complex regulatory control at each stage, as described in Section 1.3.1. Aurora kinase A (AURKA) and Polo-like kinases (PLK) are the major orchestrators of microtubule assembly during mitosis. There is significant cross-talk between AURKA and PLK1 but the end result of their activation is the initiation of microtubule assembly by recruiting and protecting microtubule-associated proteins at the sites of assembly. AURKA is a serine/threonine mitotic kinase that exerts its functions at the spindle poles to regulate the assembly and orientation of the spindle. In *Drosophila*, Bora activates AURKA to establish polarity during asymmetric cell divisions.[95] AURKA also participates in the segregation of NUMB, an inhibitor of Notch, which subsequently determines the fate of the daughter cells produced.[96] PLK1 is a serine/threonine kinase [97, 98] that recruits AURKA to centrosomes, while AURKA activates PLK1 through phosphorylation events.[99, 100, 97]

Mitosis is not a static process and the dynamics of mitosis (i.e., capture of chromosomes, alignment and congression of chromosomes, mitotic spindle orientation and determination of the axis of division) are reliant upon molecular motor proteins (i.e., the dynein motor complex) that move along and cross-link mitotic microtubules. PLKs and AURKA are necessary kinases to coordinate these dynamics. PLK1, for example, regulates the localization of NuMA/LGN/dynein complexes to the cell cortex. These complexes then position the mitotic spindle in the cell through motor forces along the cortex.[79, 101] Therefore, correct expression and interplay between mitotic kinases provides proper signaling to coordinate motor and adaptor mitotic proteins.

### 1.3.7 The dynein molecular motor and its adaptor proteins

The dynein molecular motor complex is composed of multiple subunits that, in the most simplistic terms, amounts to a long heavy chain that terminates with a large motor domain. Thus, when the dynein complex is functioning as a heterodimer, it acts as if it had 2 legs that walk along the microtubules through the catalysis of ATP using its motor domains. Adaptor proteins provide specificity to the motor in order to exert force and move the dynein complex along the microtubules to guide mitotic spindle positioning along the cell cortex.[102, 103]

Dynein binds to microtubules with the head (motor) domain while its tail binds either the cell cortex or to cargo that needs to be transported along microtubules. The dynein complex performs several functions during mitosis: 1) it regulates microtubule attachment and tension at kinetochores [104]; 2) it clears checkpoint proteins away from properly attached kinetochores to enable the transition to anaphase [105]; and 3) along with adaptors, such as the NuMA/LGN complex, dynein acts at the cell cortex in metaphase to tie and position the bipolar spindle to the cell cortex.[106, 79, 107]

Nuclear mitotic apparatus protein (NuMA) is a structural adaptor protein that localizes to the cell cortex through an interaction with Leucine-glycine-asparagine repeat protein (LGN) [108] and plasma membrane phospholipids.[109] Once at the cell cortex, NUMA/LGN sequesters dynein; together, this motor protein complex moves astral microtubules (attached to the spindle) along the cell's cortex to properly orient the mitotic spindle and establish the eventual division plane.[110, 111] The NuMA/LGN complex at the cell cortex is in equilibrium with another adaptor complex at the centrosome (RHAMM-CHICA) for occupancy with a subunit of dynein.[79] This equilibrium helps to control the

rotation of the mitotic spindle. RHAMM is an adaptor protein for dynein that helps to cross-link and stabilize the mitotic spindle.[112] Silencing of RHAMM results in a number of mitotic abnormalities, including multipolar spindle formation [112], delays in spindle assembly [113], and chromosome instability.[114] RHAMM is a substrate for PLK1 [115], AURKA [13, 113], and the BRCA1-BARD1 complex.[49, 38] Silencing of RHAMM uncouples its equilibrium with NuMA/LGN leading to overabundant dynein activity at the cell cortex and an incorrect orientation of the mitotic spindle in cells grown in tissue culture on plastic (Figure 5).[79]

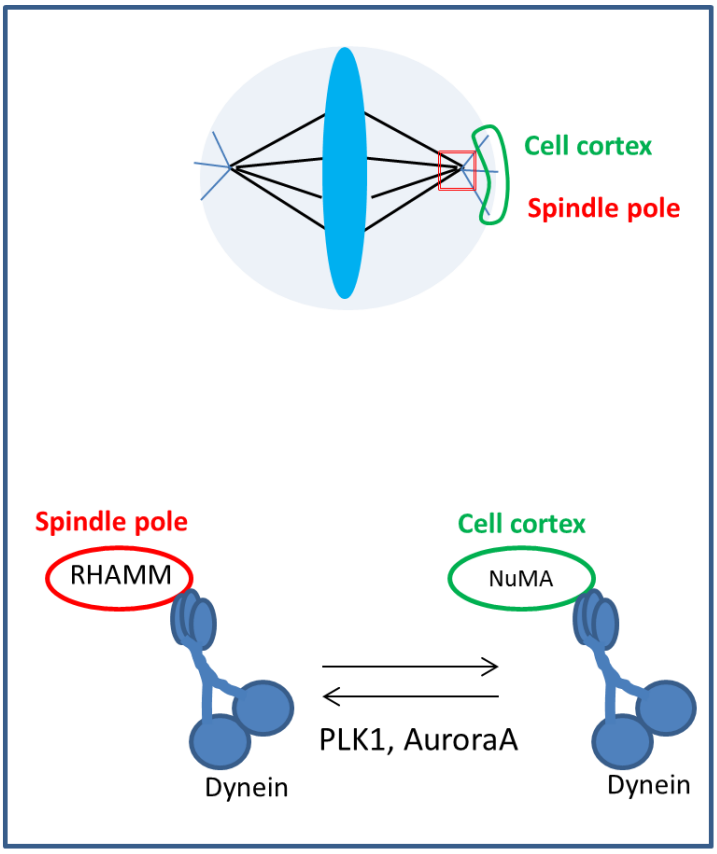


**Figure 5. RHAMM and mitotic spindle orientation.** Equilibrium is created by the RHAMM-dynein complex acting at the spindle pole and the NuMA-dynein complex at the cortex to align the spindle in the cell**.**

### 1.3.8 BRCA1 regulates RHAMM and Aurora kinase A during mitotic spindle assembly

RHAMM is a target of the BRCA1-BARD1 complex and the ubiquitination of RHAMM appears to be central to the regulation of mitotic spindle assembly through BRCA1.[49, 38] This may be due to the fact that RHAMM is critical to the activation of AURKA [113], which itself phosphorylates BRCA1 to control the G2/M transition.[64, 50] However, it is not yet clear whether the control of RHAMM through BRCA1 alters mitotic spindle orientation and the cellular fate of mammary cells, although it is clear that the reduced expression of RHAMM alters pluripotency in mouse [116] and human embryonic stem cells.[117]

### 1.3.9 Mitotic spindle orientation in the mammary gland

While directional cell division is a well-established concept in intestinal epithelia, it is not clear whether this phenomenon is pertinent to mammary epithelia. Recently, directional cell division in the mouse mammary gland has been explored by several research groups. Collectively, they found that cell division occurs planar to the basement membrane, and several pathways and mechanisms have now been delineated.

The first description of mitotic spindle positioning in the mammary gland was noted in 1988 by DJP Ferguson. In an electron microscopy study of normal human mammary tissue, this study found that most of the divisions that occurred in luminal cells showed spindles positioned perpendicular to the basement membrane (into the lumen), resulting in one daughter cell positioned luminally and another basally.[118] More recently, several studies have identified key molecular regulators for directional division of mammary cells,

including AURKA, which regulates NUMB signaling [93], PLK2 [101] and Huntingtin [119], which control NuMA/LGN complexes at the cortex.

Germline knockout mice were used to elucidate the effects of Plk2 depletion in the mammary gland.[101] Plk2 depletion resulted in increased mammary proliferation as inferred from increased ductal branching. Gene expression profiling demonstrated disrupted expression of genes involved in mitotic assembly. Subsequently, spindle misorientation, loss of apico-basal polarity and lumen filling was detected in Plk2-depleted animals.[101] Huntingtin, a gene product mutated in Huntington disease, has been shown to play a role in mitotic spindle positioning in mouse neuronal progenitors [120] and Keratin 5 promoter-driven depletion of Huntingtin produced aberrant mammary morphogenesis. Furthermore, spindle orientation in these mice was disturbed, and found to be dynein dependent. This study thus identified a role of NuMa/Lgn/dynein in targeting Huntingtin to spindle poles to establish the proper spindle orientation in mouse mammary cells.[119] Finally, AURKA expression was found to be higher in the basal mammary cells than luminal progenitors in the mouse mammary gland.[93] Expression of AURKA promoted perpendicular spindle orientation relative to the lumen, while the expression of mutant AURKA S155R resulted in spindle orientation parallel to the basal surface of the acini.[93] In this study, daughter cell fate relied on Notch signaling; when Notch signaling was active, the cell divided perpendicular to the basal surface resulting in one luminal and one myoepithelial cell while two myoepithelial cells were generated in the absence of Notch signaling.[93]

In conclusion, loss of function *BRCA1* mutations predispose human carriers to an aggressive subtype of breast cancer that shows features of primitive normal mammary cells. This subtype of breast cancer is not seen in carriers of *BRCA2* mutations, which suggests the

involvement of a tumour suppressor pathway distinct from the DNA damage response. At a molecular level, BRCA1 regulates the levels of the mitotic spindle protein RHAMM and BRCA1 is regulated by the mitotic kinase AURKA. Both of these gene products have recently been shown to regulate the process of mitotic spindle orientation, which is a critical pathway for the control of asymmetric division of tissue-specific stem cells in model organisms. To date, a role for BRCA1, if any, in the control of mitotic spindle orientation in the mammary gland is not yet described.

## 1.4 Hypothesis and Objectives

### 1.4.1 Hypothesis

BRCA1 is necessary for the correct orientation of the mitotic spindle in mammary epithelial cells, which controls their proliferation, polarization and growth arrest.

### 1.4.2 Objectives

1 Assess the extent of correlation between mitotic spindle orientation and apicobasal polarity in mammary epithelial cells.

2 Compare effects of loss of BRCA1 on spindle orientation in cell-lines cultured on plastic (2D) and in matrigel 3D cultures that normally support their polarization.

## Chapter 2: Materials and Methods

### Mammary cell lines and adherent 2D cultures on a plastic surface

All mammary cell lines were maintained at 37°C in a 5% $CO_2$ incubator and split at 70-80% confluence. The cell lines characteristics are described in Table 1.[72]

**Table 1. Mammary cell lines characteristics**

| Cell Lines | Characteristics | ER | PR | P53 | Source | Age |
|---|---|---|---|---|---|---|
| MCF10A | Non-malignant, basal by gene expression profiling (GEP) | - | - | +/- | Fibrocystic lesions | 36 |
| MCF10A-TUBA1B-RFP | Non-malignant, basal by GEP with RFP tagged TUBA1B | - | - | +/- | Fibrocystic lesions | 36 |
| MCF12A | Non-malignant, estrogen responsive | +/- | - | + | Fibrocystic lesions | 60 |
| MCF12A (shScr) | Scrambled shRNA induced by doxycycline | +/- | - | + | Fibrocystic lesions | 60 |

MCF10A (Brugge) is a non-malignant mammary epithelial cell line that was kindly provided by Dr. Eaves (BC Cancer Agency, Terry Fox Labs, Canada). MCF10A-TUBA1B-RFP, a mammary epithelial cell line with Red Fluorescent Protein (RFP)-tagged TubA1B, was purchased from Sigma-Aldrich (catalog number CLL1039). All MCF10A cell lines were cultured in Brugge media [24] as described in Table 2.

**Table 2. MCF10A Brugge media recipe**

| Reagents | [Final] | Source | Aliquot Storage (°C) |
|---|---|---|---|
| DMEM/F12 | | Gibco | +4 |
| Horse Serum | 5% final | Gibco | -20 |
| EGF | 20 ng/mL | Sigma#E9644 | -20 |
| Hydrocortisone | 0.5 µg/mL | Sigma#H088-1G | -20 |
| Cholera Toxin | 100 ng/mL | Sigma#C8052 | +4 |
| Insulin | 10 µg/mL | Sigma#I6634 | -20 |

MCF12A is a non-malignant mammary epithelial cell line derived from a patient with fibrocystic lesions (Table 1). MCF12A shScrambled (shScr) control and MCF12A shBRCA1 doxycycline (dox) inducible shRNA sub-lines were provided by Dr. Niederacher (University Hospital of Düsseldorf, Germany). Cells were cultured in Brugge media. Short hairpin RNA (shRNA) induction in these sub-lines was mediated by the addition of dox (2 μg/ml) to the media. shRNA expression was visualized with GFP expression. To silence BRCA1 expression, the cells were treated with 2 μg/ml dox 12 hrs following seeding the next day. Cells were assayed following 96 hrs of dox treatment. Successful protein knock down was confirmed by immunofluorescence and Western blot analysis.

**Primary human mammary samples from reduction mammoplasty**

Primary mammary samples were provided by Dr. CJ Eaves. They were obtained from cosmetic reduction mammoplasty surgeries performed on 7 normal individuals, with their informed consent and handled according to ethical approval from the UBC Research Ethics Board. Mammary organoids were isolated by crude enzymatic dissociation and stored at -80°C for further experiments. Primary samples used in this study are summarized in Table 3.

**Table 3. Summary of primary human mammary reduction mammoplasty samples**

| Sample | Pellet identifier |
|---|---|
| 1 | 13-11 |
| 2 | 4-11 |
| 3 | 203-01 |
| 4 | 19-11 |
| 5 | 8-13 |
| 6 | 6-14 |
| 7 | 13-14 |

**Isolation of primary mammary samples from reduction mammoplasty**

Mammary organoids were processed into a single cell suspension and separated into LP- and BC-enriched fractions by FACS, as previously described [121] (Figure 6). Mammary cells lack expression of hematopoietic (CD45) and endothelial (CD31) cell surface markers. Therefore, cells expressing these markers were excluded. LPs and BCs were then isolated based on their differential levels of expression of epithelial adhesion marker (EPCAM) and high expression of α6-integrin (CD49f).[1] There are still no known markers combinations described to separate these populations to 100% purity. Cells were processed and cultured in SF7 media as described in Table 4.

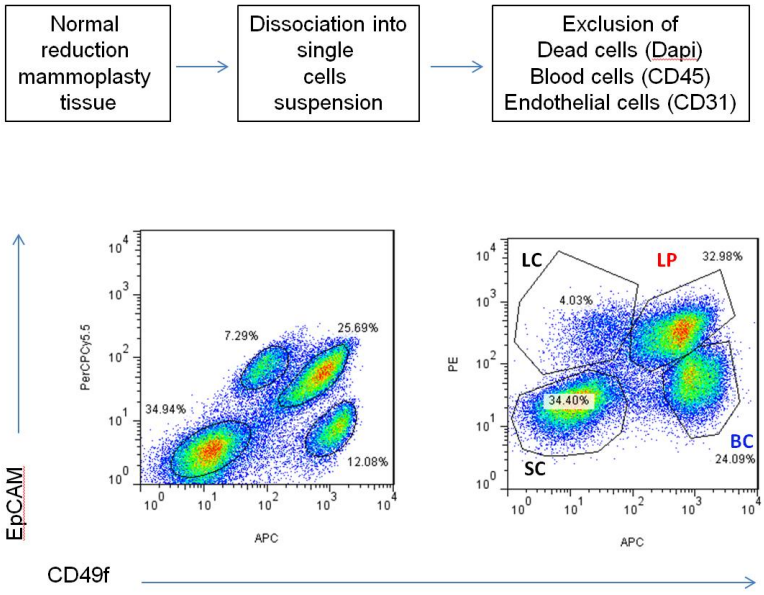


**Figure 6. FACS strategy for BC and LP fractions isolation.** Mammary cells are dissociated into single cell suspension, depleted of hematopoietic and endothelial cells and separated by flow cytometry according to EpCAM and CD49f expression to obtain progenitors enriched Basal Cells (BC) and Luminal Progenitors (LP) fraction, as well as Luminal Cells (LC) and Stromal Cells (SC).

**Table 4. SF7 media recipe**

| **Reagents** | **[Final]** |
|---|---|
| DMEM/F12/HEPES | To 100 ml |
| BSA (fraction V) | 1 mg/ml |
| Insulin | 1 µg/ml |
| Cholera toxin | 10 ng/ml |
| Hydrocortisone | 0.5 µg/ml |
| EGF | 10 ng/ml |
| Fetal bovine serum (FBS) | 5% |
| Total | 100 ml |

**Primary mammary samples from reduction mammoplasties: 3D matrigel cultures**

Primary samples were cultured in 3D, as previously described [1] and summarized in Table 3. 10,000 cells were embedded in matrigel (BD Biosciences), and placed as a drop into a well in 8 well chamber slide. The matrigel was allowed to polymerize for 15 min at 37°C. 500 µl of SF7 media was added to each well (Table 4). Cells were cultured for up to 11 days in low oxygen condition (5% $O_2$) or normal oxygen condition (21% $O_2$) at 37°C. Media was changed every two days.

**Mammary cell lines: reconstituted basement membrane (rBM) 3D assay**

Matrigel is a well extablished tissue culture system for gut, mammary and other epithelial cells that supports growth, polarity and maintenance of primitive cell populations.[122, 123, 124, 85, 24] rBM was purchased from Gibco, aliquoted and stored at -20°C. rBM cultures were performed as previously described [13], and summarized in Figure 2. rBM was thawed overnight on ice for use in 3D assays. The flat bottom 96 well plates (Falcon) were coated with 30 µl of rBM and allowed to polymerise for 30 min at 37°C, 5% $CO_2$ incubator. To achieve clonal seeding density, 2,000 mammary cells were embedded in 20 µl rBM. The plate was incubated for 30 min at 37°C, to allow rBM polymerization. Each well

was supplemented with 200 µl Brugge media. Cultures were propagated and assayed at days 5-14 of rBM cultures.

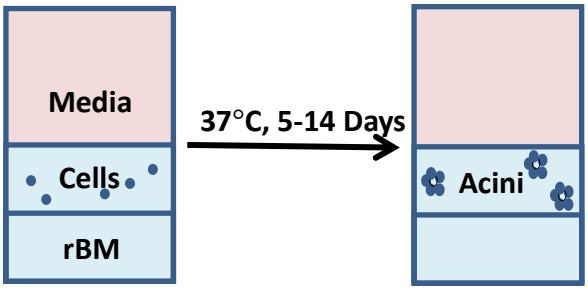


**Figure 7. Cell lines 3D cultures.** 96-well plate wells are coated with matrigel, and allowed to polimerize, mammary cells are embedded in matrigel at clonal density, and added to the well. Once matrigel polymerized, media is added to cover.

**Mammary cell lines colony forming cell (CFC) assay**

MCF10A (Brugge) cells were untreated or transduced with lentivirus to express non-hairpin shRNA (shNHP) or shRNA targeting BRCA1 (sh34BRCA1 and sh37BRCA1). After 3 days, cells were seeded at clonal density at 25 cells/well in 24 well plates and cultured for 7 days to obtain colonies. Colony formation was assessed by counting colony number.

**Lentivirus production**

Lentiviral particles were produced as previously described [13, 125]. Briefly, HEK-293FT cells were obtained from Invitrogen. Cells were maintained in 10% FBS/DMEM at 37°C, in a 5% $CO_2$ incubator and split at 70-80% confluence. Lentivirus was produced by packaging the target shRNA plasmid with packaging plasmid (psPAX2) and envelope

plasmid (pMD2.G), as described in Table 5, and the targeting sequences are provided in Table 6.

**Table 5. shRNAs used in this study**

| Plasmid | shRNA plasmid of interest | Purpose | Vector | Source |
|---|---|---|---|---|
| Target | sh34BRCA1 (puromycin selection) | Silencing BRCA1 expression | pLKO.1 | Sigma |
| Target | sh34BRCA1-GFP | Silencing BRCA1 expression | pLKO.1 | Sigma |
| Target | sh37BRCA1 (puromycin selection) | Silencing BRCA1 expression | pLKO.1 | Sigma |
| Target | sh37BRCA1-GFP | Silencing BRCA1 expression | pLKO.1 | Sigma |
| Target | sh5RHAMM (puromycin selection) | Silencing RHAMM expression | pLKO.1 | Sigma |
| Target | shNHP (puromycin selection) | NHP: Non hairpin control, does form hairpin | pLKO.1 | Addgene |
| Target | GFP | GFP alone control | pWPT-GFP | |
| Packaging | psPAX2 | Packages the virus | | Addgene |
| Envelope | pMD2.G | Viral envelope | | Addgene |

**Table 6. shRNA sequences**

| Gene/protein | shRNA sequence (5'-3') | % Knockdown[1] |
|---|---|---|
| ***BRCA1*/BRCA1** | | |
| shRNA#34 | CCGGGCCCACCTAATTGTACTGAATCTCGAGATTCAGTACAATTAGGTGGGCTTTTTG | 67 |
| shRNA#37 | CCGGGCCTACAAGAAAGTACGAGATCTCGAGATCTCGTACTTTCTTGTAGGCTTTTTG | 70 |
| ***HMMR*/RHAMM** | | |
| shRNA#5 | CCGGCGGAATCAAAGGAATCTCAAACTCGAGTTTGAGATTCCTTTGATTCCGTTTTTG | NA |

[1]Mean mRNA knockdown level in MCF7 breast cancer cell line reported by manufacturer (Sigma-Aldrich)

To produce one 10 cm plate of lentivirus, HEK-293FT cells were seeded in a 10 cm tissue culture plate in 10 mL of 10% FBS/DMEM, at the density of 4-4.5 million cells per plate. The cells were cultured in DMEM media supplemented with 10% FBS overnight and replaced with 7 ml of fresh media the next morning. In the late afternoon, cells were transfected at about 70% confluence. Transfection cocktail was prepared as described in Table 7 (Adopted from Addgene), in a polypropylene tube. Master mix (MM) was created as described in Table 8. Lipofectamine 2000 transfection reagent was added to serum-free OPTI-MEM media in a polypropylene tube. Per one 10 cm plate 232 µl of OPTI-MEM was combined with 18 µl of Lipofectamine 2000. The MM was incubated for 5 minutes (min) at room temperature (RT) and added to the transfection cocktail mix for a total volume of 500 µl (per one 10 cm plate of virus). This was mixed by swirling the tube, and incubated for 20 min at RT. The mixture was added drop wise to a 10 cm plate containing HEK-293FT cells. The plate was incubated at 37°C, 5% $CO_2$ incubator for 12-15 hrs at the designated lentiviral facility room at Child and Family Research Institute. Media was changed in the morning (5 ml of fresh 10% FBS/DMEM) to remove the transfection reagent and cells were allowed to recover for 24 hrs. Virus was harvested and transferred to a polypropylene storage tube. 5 mL of fresh media was added and cells were incubated at 37°C, 5% $CO_2$ incubator for another 24 hrs. Virus was harvested again and combined with previous harvest, to give a total of 10 ml of viral supernatant. Viral supernatant was filtered through a 0.45 µm filter to remove cells and debris. Clontech virus titrator was used to ensure sufficient virus titre. Lenti-X concentrator (Clontech, Mountain View, A) was used to concentrate the virus, which was done by adding 3.3 ml of concentrator to 10 ml of viral supernatant. This mix was stored in 4°C for 30 min for up to a week. The mix was centrifuged at 1,500 g at 4°C

for 45 min. Supernatant was discarded in bleach waste container, and the virus pellet was resuspended in 200 µl of PBS, aliquoted at 100 µl per eppendorf tube, and stored in -20°C for further use.

**Table 7. Transfection cocktail mix**

| **Transfection cocktail** | **Description** | **One reaction (one 10 cm plate)** |
|---|---|---|
| pLKO.1 shRNA | Target plasmid | 2 µg |
| psPAX2 | Packaging plasmid | 1.5 µg |
| pMD2.G | Envelope plasmid | 0.5 µg |
| OPTI-MEM | Media | To 250 µl |
| Total | | 250 µl |

**Table 8. Lipofectamine master mix (MM)**

| **Reagents** | **MM (µl) one reaction (one 10cm plate)** |
|---|---|
| OPTI-MEM | 232 |
| Lipofectamine 2000$^{TM}$ (Invitrogen) | 18 |
| Total | 250 |

**Lentiviral transduction**

Lentivirus transduction was performed as previously described.[13] shNHP was used as a negative control. MCF10A Brugge or MCF10A-TubA-RFP cells were seeded in 6 well plates at 400,000 cells/well, and allowed to grow to 60-80% confluence prior to transduction. If the confluence was not sufficient, the experiment was aborted. Cells were incubated with the viral supernatants in the presence of 8µg/ml of polybrene overnight. In the morning, the media was changed, and the cells were allowed to recover for one day. To select for successful transduction, transduced cells were exposed to 1 µg/ml puromycin (GIBCO); untreated cells died in the presence of puromycin after 5 days.

**Western blot assay**

Western blot assay was performed as previously described.[13] At 70-90% confluence, cells were collected by trypsinizing with 0.25% trypsin and washed once with PBS. Cells were counted using a hemocytometer. 2 X $10^6$ cells were pelleted and lysed in 200µl of RIPA buffer with protease inhibitor (Roche 04-693-124-001). Cells were lysed for 30 min at 4°C and then mechanically disrupted by passing the lysates through a 25G 5/8 syringe five to ten times. Lysates were centrifuged for 30 min at 4°C at 20,000 g, and supernatants were transferred to new tubes to remove detergent insoluble proteins. Protein concentration was measured with BCA protein assay kit as per manufacturer's instructions (Thermo scientific). Each reaction was run in triplicate. Six Bovine Serum Albumin (BSA) standards and one lysis buffer (negative control) were used to obtain the protein concentration of the samples. A standard curve was plotted with absorbance reading at OD562 on the y-axis and standard concentration on the x-axis, and this equation was used to determine protein concentration. Proteins were denatured by adding 3x loading buffer to the samples and boiled at 95°C for 5 min. Subsequently, proteins were resolved by sodium dodecyl sulfate-polyacrylamide gel electrophoresis (SDS-PAGE) on an 8% gel and transferred onto nitrocellulose membrane using the Bio-Rad Semi dry transfer apparatus. Transfer was performed at 4°C overnight using 28 V. After washing once with TBSTween buffer, the membrane was blocked with 3% milk/TBSTween for 1 hr at RT. The membrane was washed three times in TBST for 10 min each prior to incubation with primary antibodies (Table 9) diluted in 3% BSA/TBSTween for 1 hr at RT or overnight at 4°C. Blots were washed 3 times with TBST for 10 min and incubated with HRP-conjugated labeled secondary antibodies (Sigma) 1 hr at

RT. A final wash was done with TBST (3 times/10 min each). Proteins were detected using an ECL Kit (Thermo).

**Table 9. Antibodies used for western blot analysis**

| Antibodies | Supplier | Source | Dilution | Band(kDa) |
|---|---|---|---|---|
| BRCA1 | Cell Signaling | Rabbit | 1:100 | 220 |
| β-Actin | Sigma A5060 | Rabbit | 1:2000 | 42 |
| GFP | Abcam ab1218 | Mouse | 1:1000 | 25 |
| RHAMM | Epitomics | Rabbit | 1:1000 | 85 |
| Secondary antibody conjugated to HRP | Sigma | Mouse | 1:20,000 | |
| Secondary antibody conjugated to HRP | Sigma | Rabbit | 1:20,000 | |

**Immunofluorescence staining in 2D**

Cells were seeded onto glass coverslips at 50,000 cells/well in a 24 well plate. The next day, cells were washed 2 times for 5 min with PBS and fixed with 4% paraformaldehyde (PFA) for 20 min at RT. Cells were washed with PBS 2 times and permeabilized with 0.5% Triton X-100/PBS for 15 min at RT. Alternatively, cells were fixed and permeabilized with cold methanol in -20°C for 20 min. Cells were washed with PBS 2 times for 5 min each. Cells were blocked in 2% BSA/0.1% Triton X-100/PBS blocking buffer (Block) for 30 min at RT. Coverslips were taken out onto the parafilm covered surface, or stained in the well with desired antibodies. All antibodies were diluted in Block (Table 10). Cells were immunostained by incubating with relevant primary antibodies for 1 or 2 hrs at RT, followed by 3 washes in PBS for 5 min each. Secondary antibody was incubated for 1 hr at RT, protected from light, followed by 3 washed in PBS for 5 min each. Finally, a water wash was performed for 5-10 min to remove the salts in PBS. Coverslips were mounted with ProLong Antifade Reagent with 4,6-diamidino-2-phenylindole (DAPI),

to delineate the DNA (Invitrogen). Images were acquired and analyzed on Olympus FV10i confocal microscope, under a 60x immersion oil objective. Fluorescent images were processed with Olympus FV10i Fluoview software.

**Table 10. Antibodies used for immunofluorescence analysis in 2D and 3D**

| Antibodies | Supplier | Host | 2D dilutions | 3D dilutions |
|---|---|---|---|---|
| Alexa Fluor 647 goat anti mouse IgG; Alexa Fluor 647 goat anti rabbit IgG; Alexa Fluor 594 goat anti mouse IgG; Alexa Fluor 594 goat anti rabbit IgG; Alexa Fluor 488 goat anti mouse IgG; Alexa Fluor 488 goat anti rabbit IgG | Invitrogen | | 1:2000 | 1:200 |
| TubB-Alexa Fluor 647 | Cell Signaling | Rabbit | 1:2000 | 1:200 |
| Rad51 | Santa Cruz | Rabbit | 1:500 | N/A |
| TubG1 | Sigma Aldrich | Mouse | 1:2000 | 1:100 |
| Pericentrin | Covance | Rabbit | NA | 1:50 |
| CD49f | Millipore | Mouse | NA | 1:200 |
| BRCA1 | SD118, Calbiochem | Mouse | 1:10 | NA |

**Immunofluorescence staining in 3D**

Cells were washed 3 times with PBS. GFP-tagged acini were fixed in 4% PFA for 1.5 hrs at RT. Acini lacking GFP expression were fixed in cold methanol at -20°C for 30 min and up to 1 hr. Fixative reagent was removed from the wells, and the wells were air-dried briefly. The sample was blocked for 1.5 hrs at RT. Primary antibody (Table 9), diluted in Block, was applied and incubated at 4°C overnight. Antibody was removed the next day and the sample was washed with PBS 3X. Secondary antibody was applied, and incubated at 4°C for 4 hrs. The sample was washed with PBS three times and once with sterile water. The sample was mounted in ProLong Antifade Reagent with DAPI, to delineate the DNA (Invitrogen), and allowed to fully dry before imaging on confocal microscope.

**DNA damage assay Rad51 analysis in 2D**

Cells were seeded at 50,000 cells/well density in a 24 well plate. The following day, cells were assayed at about 70% confluence. Cells were treated with 80 µg/ml of mitomycin C (2 hrs at 37°C) to induce DNA crosslinking and fixed in 4% PFA for 20 min at RT. Cells were then permealized with 0.5% triton/PBS for 15 min RT and blocked for 20 min at RT with Blocking buffer. Cells were incubated with Rad51 antibody (Table 10) for 1 hr at RT followed by 3 washes with PBS. Secondary antibody was applied for 1 hr at RT. Cells were treated with NucBlue Live cell stain (Molecular probes) to mark the nuclei, and imaged on the ImageXpress microscope. Only Rad51 foci in the nuclei were assessed in this analysis, by counting the presence or absence of nuclear foci.

**Mitotic analysis of fixed cells in 2D**

Mitotic abnormalities were assessed in fixed samples. Aberrant mitotic spindles were defined as multipolar spindles (spindles with 3 or more poles, as delineated by tubulin stain) and lagging or unattached chromosomes (chromosomes not separated completely at anaphase, any chromosomes attached at the wrong side of spindle, or non-attached, floating chromosomes, as delineated by DAPI stain). Cells were imaged on confocal microscope and percent abnormalities were calculated.

**Post-mitotic analysis of fixed cells in 2D**

Post-mitotic abnormalities were assessed in cells fixed with 4% PFA. Multinucleated cells were defined as any cell with two or more nuclei (as indicated by DAPI staining) in one cytoplasm (as delineated by tubulin staining). Cells with micronuclei were defined as

any cell with unattached nuclear material, as stained by DAPI. Cells were imaged on confocal microscope and percent abnormalities were calculated.

**Mitotic spindle orientation in fixed and live cells in 2D**

Quantitation of mitotic spindle orientation was performed on mitotic cells fixed, stained and then imaged on the confocal microscope. Cells were separated by mitotic phases: all mitosis, metaphase only, and anaphase and telophase. Prometaphase cells were excluded. Only normal mitotic spindles were assessed in this experiment, while all the abnormal mitotic figures were excluded (i.e., multipolar spindles, unattached chromosomes, or anything else looking ambiguous). Cell confluence was about 50-80% to allow optimal cell growth. Normally, mitotic spindles are positioned about parallel to the growth surface, which is 0-10° to the coverslip, while the angle is increased in abnormal spindle positioning.[79] Z-stacks of the mitotic spindles were taken, and rotated 90°. The angle of spindle orientation, with respect to the coverslip, was measured using the Olympus software. Percent abnormal spindle orientation was calculated.

Living cells were imaged on the ImageXpress Micro High Content Screening System (Molecular Devices Inc.) and mitotic spindle rotation relative to the growth surface was quantified in metaphase cells. Cells were imaged for up to 10 hours at 10 minute intervals. Rotating spindles were identified by the positioning of the spindle poles, which would change in the vertical axis during metaphase.

**Acinar polarization in fixed mammary primary cells and cell lines in 3D**

Acini were defined as spheroid with at least 50 cells, as approximated by nuclear DAPI stain. All acini were imaged on confocal microscope with 60X oil objective. Z-stacks were obtained and the middle sections were used to assess polarization in 3D. Acinar polarization was evident from apical positioning of the centrosomes, as indicated by staining with TUBG1 or Pericentrin, and the basal deposition of integrins, as indicated by staining with CD49Ff.

**Spindle orientation measurement in fixed mammary primary cells and cell lines in 3D**

Acini were defined as at least 50 cells, as approximated by nuclear DAPI stain. All acini were imaged on confocal microscope with 60X oil objective. Z-stacks were obtained and the middle sections were used to assess polarization in 3D. Mitotic cells in metaphase, anaphase and telophase were imaged. Care was taken to ensure that spindle orientation was quantified in the central sections of the acini, so that parallel/planar (mitotic spindle orientated along the basal surface of the acini) versus non-planar (spindle oriented perpendicular to the surface of the acini) could be distinguished in 3D space. We set a cut off for planar (parallel) spindle orientation at angles between 0-30°, and non-planar (perpendicular) spindle orientation was set at angles between 61-90°. Abnormal mitosis was excluded from the analysis. Mitosis was assessed by mitotic phases to exclude the possibility of spindle rotation in metaphase. Three groups were created: 1) metaphase, anaphase and telophase (all mitosis); 2) metaphase only; or, 3) anaphase and telophase. Percent of cells with parallel divisions was calculated.

**Mitotic arrest analysis in fixed mammary primary cells and cell lines in 3D**

Acini were imaged on confocal microscope. Mitoses were noted in acini, and the percentage of acini with mitotic cells was calculated at late days of rBM cultures.

**Confocal microscopy**

Fixed cells were imaged with 60X 1.2NA oil objective on the Olympus Fluoview FV10i (Olympus) confocal microscope. Image z-stacks consisted of a minimum 3 and maximum 25 optical sections, with a spacing of 1.0 μm through the cell or acinar volume were imaged. One shot pictures were taken when appropriate. Maximum intensity projection of the fluorescent channels was done with the Olympus Fluoview software.

**Light microscopy**

Images of unfixed acini were taken throughout the course of 3D cultures with the Olympus CKX41 microscope at either 4X or 20X objective lens.

**Live cell microscopy**

Cells were seeded at 10,000 cells/well and incubated at 37°C in a 5% $CO_2$ incubator overnight. The sample was imaged the next day. Hoechst (1μg/μl) was applied to the cells to delineate DNA, for 30 min at 37°C. Cells were washed 3 times with Brugge media. Finally, Brugge media was added to the very top of each well. The cells were imaged immediately. The ImageXpress Micro High Content Screening System (Molecular Devices Inc.) was used

for live cell imaging. Cells were imaged every 10-12 min for up to 16 hrs at 37°C in a 5% $CO_2$ environmental chamber. Images were acquired with either 20X or 40X objective.

**Statistics**

Differences between two samples were determined with either equal or unequal variance (to account for the fact that sample size was not equal), two-tailed Student's t-test. Unequal variance t-test was used in Figure 8G (shRHAMM condition only: two experiments for RHAMM depletion were compared with at least 3 shNHP experiments) and Figure 11G-H . Equal variance t-test was used in all other cases. The results were considered significant at $p < 0.05$. Error bars represent the standard error of the mean (SEM).

## Chapter 3: Results

### 3.1 Silencing BRCA1 expression in 2D cultures of human mammary MCF10A cells alters spindle orientation with mitotic and post-mitotic consequences.

To model the reduced expression that results from loss of function *BRCA1* mutations and study the effects of this manipulation on the orientation of cell divisions in polarized mammary epithelia, I transiently transduced non-malignant MCF10A-TubA1B-RFP (endogenous tubulin, tagged with RFP) cells with lentiviral short hairpin RNA (shRNA) constructs targeted against BRCA1 mRNA. Two redundant (sh1BRCA1 or sh2BRCA1) constructs were used to silence BRCA1, and a non-hairpin shRNA control (shNHP) and untreated (UT) MCF10A cells served as negative controls. Western blot analysis performed on extracts of cells transduced two days previously showed a reduction in BRCA1 protein expression, relative to cells treated with the shNHP vector or UT control cells (Figure 8A). To determine whether this also caused a functional loss of BRCA1 activity, I assessed the formation of Rad51 complexes following mitomycin C-induced damage.[54] The results showed that the sh1BRCA1 or sh2BRCA1-transduced cells contained 5.5 and 9.7-fold fewer Rad51 foci relative to NHP-treated cells respectively ($p=0.01$, Figure 8B).

Next, I examined the effect of BRCA1 silencing on mitotic spindle assembly and the integrity of cell division in MCF10A cells. Immunofluorescent (IF) analysis was used to identify mitotic and post-mitotic abnormalities in fixed cells. These included alterations in the architecture of the mitotic spindle (demarked by the endogenous RFP-TubA1B) and in the proper alignment of chromosomes at the metaphase plane, segregation at anaphase, or

micronucleus and multinucleate formation in interphase (visualized by the DAPI counterstain). Representative images of a normal, bipolar mitotic spindle (shNHP treated cells) and abnormal, multipolar spindles (sh1BRCA1 and sh2BRCA1 treated cells) are shown in the top panel in Figure 8C. Overall, the stable silencing of BRCA1 did not result in an increase in the levels of multipolar spindles, defined as mitotic spindles with 3 or more poles ($p=0.52$, Figure 8C). However, BRCA1 silencing did result in a significant increase in the levels of lagging chromosomes during anaphase ($p <0.05$), which correlated with an increase in the frequency of multinucleate cells, defined as a cell with 2 or more nuclei in one cellular body (delineated by RFP-TubA1B), and cells with micronuclei, defined as cells with unattached nuclear material (delineated by DAPI) (Figure 8D).

The silencing of BRCA1 did not significantly impact multipolar spindles but did augment the frequency of lagging chromosomes, which implies a defect(s) during chromosome congression or segregation that may result through defects in the spindle assembly checkpoint [126, 127] or through spindle misorientation.[128] A role for BRCA1, along with p53, in the spindle assembly checkpoint has been described [129] but, to date, a role for BRCA1 in spindle orientation is not known.

During growth in tissue culture, adherent cells typically orient the mitotic spindle, and the plane of cell division, parallel to the growth surface, or coverglass.[79] To study a role for BRCA1 during spindle orientation, I examined whether or not the bias for a parallel division was altered when BRCA1 was silenced in MCF10A cells. To do so, MCF10A cells were fixed and confocal images of metaphase and anaphase cells through the Z-plane were

collected and then rotated by 90° to provide a view of the mitotic spindle (RFP-TubA1B), chromosomes (DAPI) and spindle poles (TUBG1). This view along the coverslip allows the angle of mitotic spindle rotation (i.e., the angle of a line connecting the 2 spindle poles relative to the coverglass) to be determined (Figure 8E). As a positive control, I assessed cells in which RHAMM had been silenced, as this has been published to alter spindle orientation [79]. Spindle angles were measured in 10° increments, between 0° and 90°, relative to the coverslip. In NHP control cells, >85% of mitotic spindles were oriented at an angle of <10° relative to the coverglass, which I assigned as a normal spindle orientation (Figure 8F). The stable silencing of BRCA1, however, resulted in a significant increase in the percentage of cells with abnormal mitotic spindle orientation relative to the coverslip ($p < 0.01$, Figure 8G).

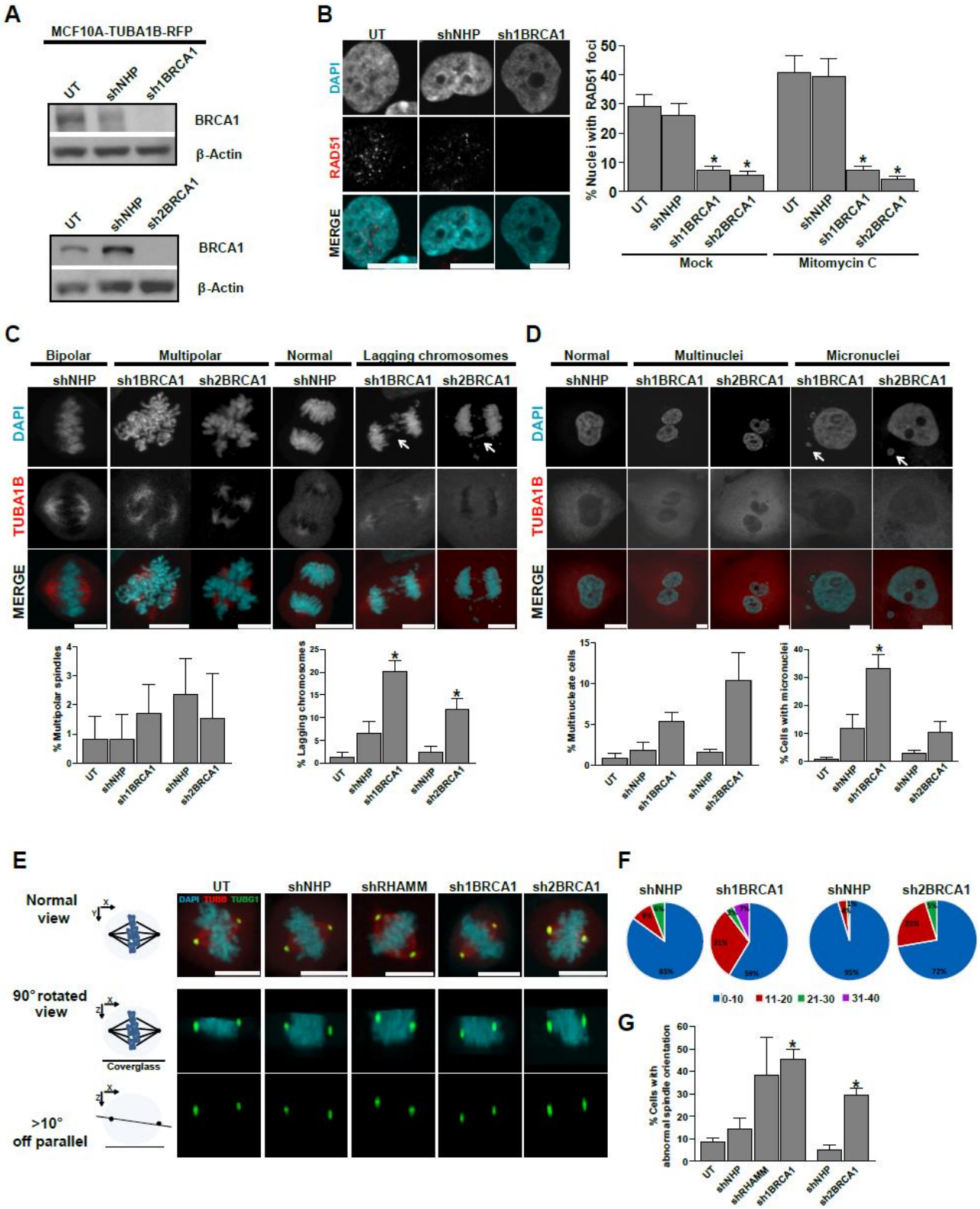
A
MCF10A-TUBA1B-RFP
UT
shNHP
sh1BRCA1
BRCA1
β-Actin
UT
shNHP
sh2BRCA1
BRCA1
β-Actin
B
UT
shNHP
sh1BRCA1
DAPI
RAD51
MERGE
% Nuclei with RAD51 foci
Mock
Mitomycin C
C
Bipolar
Multipolar
Normal
Lagging chromosomes
shNHP
sh1BRCA1
sh2BRCA1
DAPI
TUBA1B
MERGE
% Multipolar spindles
% Lagging chromosomes
D
Normal
Multinuclei
Micronuclei
% Multinucleate cells
% Cells with micronuclei
E
Normal view
90° rotated view
Coverglass
>10° off parallel
UT
shNHP
shRHAMM
sh1BRCA1
sh2BRCA1
F
shNHP
sh1BRCA1
shNHP
sh2BRCA1
0-10
11-20
21-30
31-40
G
% Cells with abnormal spindle orientation
shRHAMM

**Figure 8. BRCA1 silencing abrogates DNA damage response, increases mitotic and post- mitotic abnormalities and alters mitotic spindle orientation in MCF10A cells.**

**A.** MCF10A-TubA1B-RFP mammary cells that encode a red fluorescent tagged protein in the endogenous alpha-tubulin 1B (TubA1B-RFP) were untreated (UT) or infected with lentivirus encoding either a non-hairpin shRNA control (shNHP), a shRNA targeting BRCA1 (sh1BRCA1) or an alternate shRNA targeting a different region in BRCA1 (sh2BRCA1). At 48 hrs post-transfection, cell lysates were collected and the levels of BRCA1 protein were analyzed by Western blotting. Actin served as a loading control.

**B.** BRCA1 silencing attenuates the DNA damage response. At 72 hrs post-transduction, cells were treated with either water (Mock) or with 80 µg/ml mitomycin C for 2 hrs at 37°C, fixed with 4% paraformaldehyde (PFA) and immunostained for Rad51 and a nuclear counterstain DAPI. Representative images (from mitomycin treated condition) of Rad51 foci are shown in the left panel. The percentage of nuclei with Rad51 foci are quantitated in the graph. 141 ± 31 cells were analyzed per treatment group. Error bars represent the standard error of the mean (SEM) for triplicate measurements. Asterisk: $p<0.05$. Scale bars are 10 µm.

**C.** BRCA1 silencing disrupts mitotic integrity. At 72 hrs post- transduction, cells were fixed and assessed for mitotic abnormalities using endogenous TubA1B-RFP and DAPI. Top panel shows representative images of a bipolar mitotic spindle (shNHP) and multipolar mitotic spindles (sh1BRCA1 and sh2BRCA1), as well as a normal anaphase (shNHP) and anaphase cells with lagging chromosomes as indicated by the arrows (sh1BRCA1 and sh2BRCA1). The percentage of cells with multipolar spindles and lagging chromosomes is quantitated in the bar graphs. 161 ± 43 cells were analyzed per treatment group. Error bars represent SEM for at least triplicate measurements. Asterisk: $p<0.05$. Scale bars are 10 µm.

**D.** BRCA1 silencing induces aneuploidy. At 72 hrs post- transduction, cells were fixed and assessed for post-mitotic abnormalities. Top panel shows representative images of a normal interphase cell (shNHP), a multinucleate cell (defined as cells containing 2 or more nuclei within the cell body delineated by TubA1B-RFP) and a cell with evidence of micronuclei, indicated by arrows (sh1BRCA1-GFP and sh2BRCA1). The percentage of multinucleate cells and cells with micronuclei is quantitated in the bar graphs. 183 ± 35 cells were analyzed per treatment group. Error bars represent SEM for at least triplicate measurements. Asterisk: $p<0.05$. Scale bars are 10 µm.

**E.** BRCA1 silencing alters spindle orientation. At 72 hrs post- transduction, cells were fixed and assessed for mitotic spindle orientation relative to the growth surface. The mitotic spindle (TubA1B-RFP) was captured by confocal microscopy through the cell body, at 1 µm slices in Z-direction. Image stacks were rotated 90° in Olympus software, to allow the visualization along the growth surface (y-plane in cartoon). Spindle orientation was determined by measuring the angle relative to the cover glass to the line connecting the mitotic spindle poles. Scale bars are 10 µm.

**F.** BRCA1 silencing alters spindle orientation. Mitotic spindle angles distribution was plotted and the cut off for the normal angle positioning relative to the cover glass was determined. Angle distribution in shNHP and sh1BRCA1-GFP and shNHP and sh2BRCA1 treated cells is shown in the pie charts. Three independent experimental measurements were performed for this analysis.

**G**. BRCA1 silencing alters spindle orientation. Normal spindle orientation was defined as <10° off-parallel. The percentage of cells with an abnormal spindle orientation (angle more than 10° relative to coverslip) is quantified in the bar graph. 62 ± 27 mitotic cells were analyzed per treatment group. Error bars represent the SEM for at least triplicate measurements. shRHAMM (N=2). Asterisk: $p<0.05$.

### 3.2. BRCA1 silencing increases mitotic spindle rotation and disrupts mitotic integrity.

Mitotic spindle assembly and orientation are dynamic processes and the stable expression of RFP-TubA1B at the endogenous TubA1B locus in MCF10A cells enabled these processes to be analyzed in living cells in real-time (Figure 9A). This has the advantage of allowing post-mitotic effects to be identified directly in variously pre-treated cells showing spindle orientation defects rather than having to rely on correlative evidence obtained from different aliquots of fixed cells. Accordingly, MCF10A-TubA1B-RFP cells were first treated with one of two redundant shRNAs targeting BRCA1, or a NHP control, or were left UT and, after 72 hours, were followed overnight with an ImageXpress Micro high content analysis system, which regulates $CO_2$ and temperature. Mitotic cells were identified and kinetic measurements were performed based upon microtubule structures (TubA1B-RFP) and a Hoescht counterstain for DNA. As mitotic cell viability can be negatively impacted by the concentration of the Hoechst counterstain and the imaging process, I assessed the maximal length of imaging time during which parental MCF10A-TubA1B-RFP cells successfully complete mitosis. I found that the levels of mitotic cell death, or catastrophe, were minimal for the first 10 hours of imaging (Figure 9B). Thus, I followed MCF10A-TubA1B-RFP cells for 10 hours and measured: 1) the time necessary to

assemble a mitotic spindle (based upon TubA1B-RFP); 2) the necessary time to complete mitoses (based upon the abscission of the furrow); 3) the presence or absence of mitotic spindle rotation (relative to the coverslip); and, 4) the post-mitotic consequences for spindle rotation, including normal progeny, cytokinesis failure and/or binucleate cells, micronuclei, cell death.

To measure the duration of spindle assembly, the time between chromosome condensation (prophase) and the alignment of chromosomes at the metaphase plate was determined. This showed no significant difference between the treatment groups (29.8 ± 5.9 mitotic cells analyzed per group, Figure 9D). UT cells and NHP cells required 14.7 ± 5.7 mins and 14.5 ± 2.4 mins, respectively, while cells in which BRCA1 was silenced required 23.7 ± 5.5 mins (sh1BRCA1) and 18.9 ± 2.8 mins (sh2BRCA1), respectively, to assemble a mitotic spindle (data pooled from 2 experiments for UT cells, and from 3 experiments for the other groups). To investigate the duration of mitosis, the time between chromosome condensation (prophase) to the abscission of the cleavage furrow was measured (28.5 ± 4.7 mitotic cells analyzed per group). Again, no significant differences were detected (Figure 9E). UT cells and NHP shRNA required 38.5 ± 5.3 mins and 43.6 ± 2.6 mins, respectively, while cells in which BRCA1 was silenced required 56.4 ± 12.4 mins (sh1BRCA1) and 44.3 ± 6.2 mins (sh2BRCA1), respectively (data from 2 experiments for UT cells, and 3 experiments for the other groups). While the silencing of BRCA1 expression did not seem to impact the transit time through mitosis, I did observe a dramatic and significant increase in the frequency of mitotic cells that underwent a spindle rotation phenotype ($p<0.01$, Figure 9F). This result is consistent with those obtained on fixed samples. In living cells, spindle

rotation was defined as a deviation of the spindle axis from parallel to the coverslip as illustrated in the representative images (Figure 9C). Provocatively, many of the cells that underwent a spindle rotation phenotype resolved with lagging chromosomes during anaphase and post-mitotic micronuclei (Figure 9C). When I quantitated post-mitotic defects, I found that the silencing of BRCA1 resulted in an increase in cytokinesis failure and/or binucleate cells, micronuclei, and post-mitotic cell death (Figure 9G).

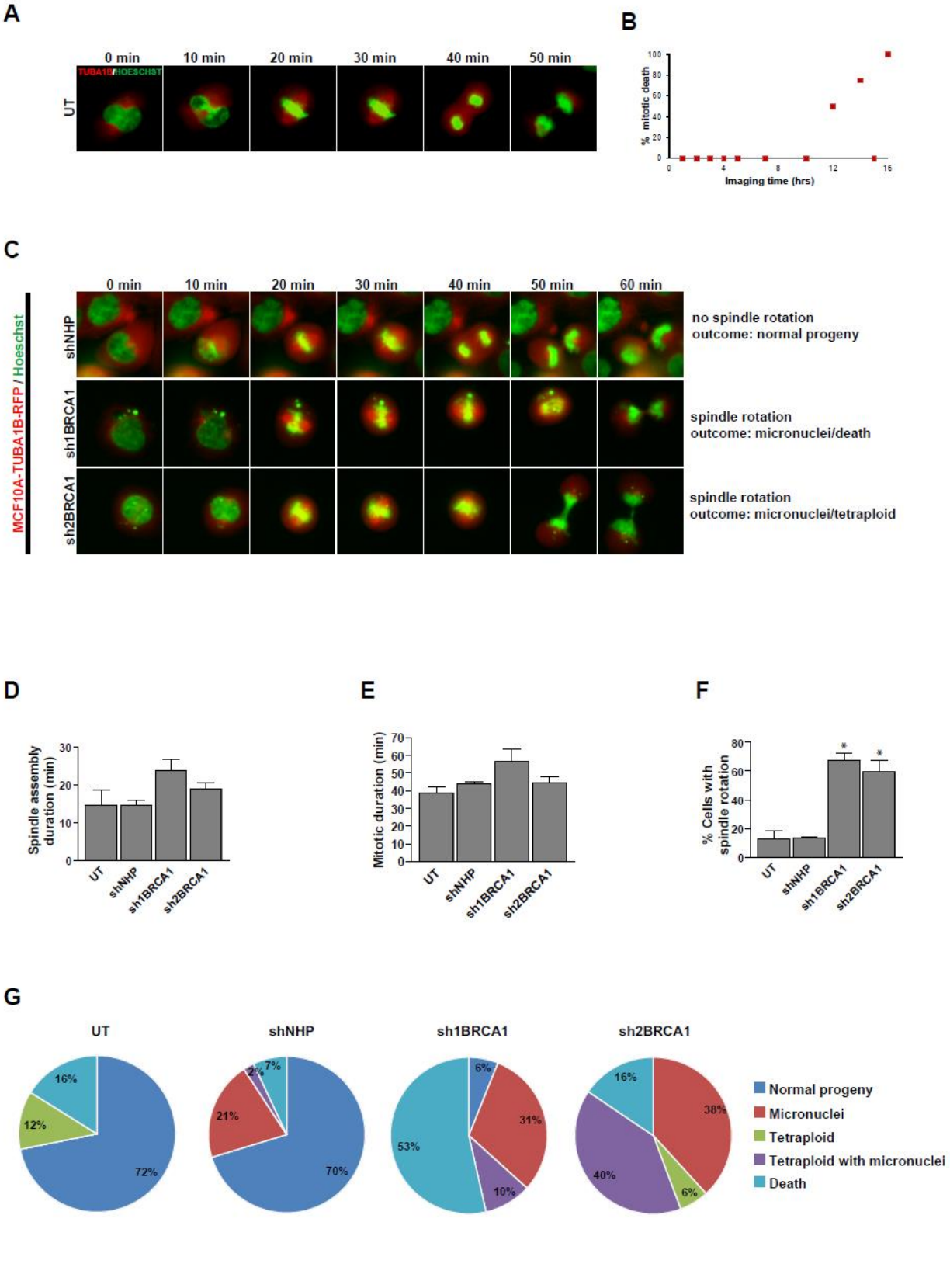
A
0 min
10 min
20 min
30 min
40 min
50 min
TUBA1B/HOESCHST
UT
B
% mitotic death
Imaging time (hrs)
C
0 min
10 min
20 min
30 min
40 min
50 min
60 min
MCF10A-TUBA1B-RFP / Hoeschst
shNHP
sh1BRCA1
sh2BRCA1
no spindle rotation
outcome: normal progeny
spindle rotation
outcome: micronuclei/death
spindle rotation
outcome: micronuclei/tetraploid
D
Spindle assembly duration (min)
UT
shNHP
sh1BRCA1
sh2BRCA1
E
Mitotic duration (min)
F
% Cells with spindle rotation
G
UT
shNHP
sh1BRCA1
sh2BRCA1
16%
12%
72%
2%
7%
21%
70%
6%
31%
53%
10%
16%
38%
40%
6%
Normal progeny
Micronuclei
Tetraploid
Tetraploid with micronuclei
Death

**Figure 9. Silencing of BRCA1 alters mitotic outcome through increased mitotic spindle rotation in cells grown on plastic.**

**A.** MCF10A-TubA1B-RFP (UT) cells were imaged for 16 hrs at 10 min intervals. The mitotic spindle was delineated with endogenous TubA1B-RFP and chromosomes with Hoechst stain.

**B.** In the untreated group, mitotic cells were followed at each time point to determine the percentage of cell death that may be due to the imaging conditions.

**C.** MCF10A-TubA1B-RFP cells were transduced with lentivirus encoding either a non-hairpin shRNA control (NHP), a shRNA targeting BRCA1 (sh1BRCA1) or an alternate shRNA targeting a different region in BRCA1 (sh2BRCA1). 72 hrs post-transduction, cells were imaged live for 10 hrs at 10 min intervals. The mitotic spindle was delineated with endogenous TubA1B-RFP and chromosomes with Hoechst stain. Representative images of shNHP, sh1BRCA1 and sh2BRCA1 are shown.

**D.** Mitotic spindle assembly duration was measured from onset of prophase to metaphase as defined by chromosomes condensation and chromosomes alignment at metaphase, respectively. Time to complete mitotic spindle assembly (min) is shown for UT, shRNA, sh1BRCA1 and sh2BRCA1 treated cells in the bar graph with error bars representing the SEM for at least 3 experimental measurements.

**E.** Mitosis duration was defined as time to complete mitosis from the onset of prophase (chromosomes condensed) to the end of telophase (onset of the cleavage furrow). Time to complete mitosis (min) is shown for UT, shNHP, sh1BRCA1 and sh2BRCA1 treated cells is shown in the bar graph. Error bars represent the SEM for at least 3 experimental measurements.

**F.** The mitotic spindle rotation was measured in all treatments. Percentage of cells with mitotic spindle rotation is quantified in the bar graph with error bars representing the SEM for at least one experimental measurement. Asterisk: $p<0.05$.

**G.** Mitotic consequences were quantified in all treatments. Percentage of normal cells, tetraploid cells, cells with micronuclei and cellular death for UT, shNHP, sh1BRCA1, sh2BRCA1 is shown in the pie chart.

### 3.3. Silencing BRCA1 in MCF10A impairs their clonogenic activity.

Given the immediate and significant consequences of BRCA1 silencing in MCF10A cells, the consequences of this on their clonogenic capacity was also measured. The results showed a significant reduction in clonogenic activity in the test cells transfected with shRNA constructs that silence BRCA1 as compared to controls (following the seeding of 25 MCF10A cells per well, colony formation was reduced from 40.8 ± 5.9 in assays of UT cells and 27.0 ± 8.1 for NHP cells to 10.2 ± 3.2 and 8.3 ± 4.5 when the expression of BRCA1 was silenced, $p < 0.05$, Figure 10).

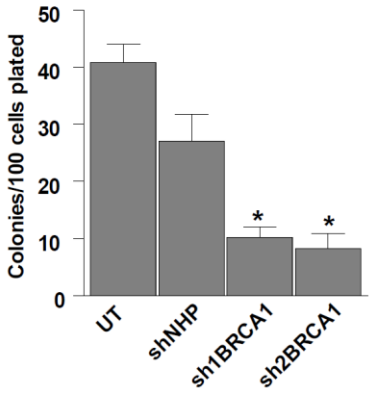


**Figure 10. Silencing BRCA1 reduces clonogenic activity in MCF10A cells.**
MCF10A cells were untreated (UT) or infected with lentiviruses encoding either a non-hairpin shRNA control (shNHP), or shRNA targeting BRCA1 (sh1BRCA1 and sh2BRCA1). 48 hrs post-transfection, CFC assays were performed at 25 cells/ well in a 24 well plates. After 7 days in culture, colonies were defined at 50 or more cells. Number of colonies formed per 100 cells seeded is quantified in the bar graph with error bars representing the SEM for at least three experimental measurements. Total colonies assessed in three experiments were 168, 142, 46, and 26 for UT, shNHP, sh1BRCA1 and sh2BRCA1 treated conditions. Asterisk: $p<0.05$.

### 3.4. Acinar morphogenesis, polarization and mitotic spindle orientation require BRCA1.

When clonally propagated in 3D rBM culture, MCF10A cells form apicobasal polarized acinar structures that growth arrest after 10-14 days in culture.[24] In other epithelia, the establishment of these polarized structures requires the spatial control of cell division; that is, the mitotic spindle is restricted to planar divisions, which ensures the stability of the polarized structure.[110, 130] It was therefore of interest to investigate the effect of BRCA1 silencing in MCF10A cells in 3D cultures.

Following the silencing of BRCA1, or treatment with NHP control shRNA, MCF10A cells were seeded at clonal density in rBM and their growth, polarization, and proliferation were followed after one week or two weeks in culture. Representative images of the size and shape of the cellular structures produced are provided in Figure 11A. UT and NHP cells formed spherical acinar structures, and the silencing of BRCA1 both reduced the total number of structures obtained but also produced larger ($p < 0.005$) and less circular structures ($p < 0.02$) when these structures formed (Figure 11B). In addition, I found that the control cells formed spherical, lumenized acini with apical centrosomes (visualized by TUBG1 IF) and basal deposition of CD49f, whereas the larger cellular structures formed when BRCA1 was silenced did not show this marker of polarization and were poorly, if at all, lumenized (Figure 11C). After 10-14 days of culture, very few of the control-treated acini contained mitotic figures whereas a significantly higher number of mitotic acini were observed in the cultures of BRCA1-silenced cells (Figure 11D). Indeed, through the analysis

of apicobasal polarity and mitotic acini, it became evident that directional mitoses were also reduced in cellular structures generated following the silencing of BRCA1 (Figure 11F).

To assess planar cell division, cellular or acinar structures were fixed following 9-14 days of 3D growth in rBM. To determine the axis of division, the mitotic spindle was localized by tubulin immunofluorescence and the DNA was counterstained with DAPI. Confocal images were acquired through the volume of the structures and care was taken to ensure that spindle orientation was quantified in the central sections of the acini, so that parallel (mitotic spindle orientated planar, along the plane of the basal surface) versus perpendicular (spindle oriented into the plane of the basal surface) could be distinguished in 3D space. Similar to the measurement of spindle orientation relative to the coverslip, I measured the angle of the line connecting the spindle poles relative to the angle of the basal cell surface, with an angle of 0°-30° being classified as planar (parallel), and 61°-90° classified as perpendicular (Figure 11E cartoon). Representative images of planar and perpendicular cell division in anaphase cells (spindle is delineated with TubA1-B and nuclear material with DAPI) are shown at the middle cross-section of the acini (Figure 11E). I first measured the spindle angles within UT and NHP mitotic cells, focusing on cells in metaphase, anaphase, and telophase, excluding mitotic cells with multipolar spindles or lagging chromosomes in this analysis and using a cut-off of 0°-30° to identify planar divisions (Figure 11F).

This analysis revealed that the vast majority of cell divisions (>80%) were planar in UT and NHP cells (n=34 and n=14 mitotic cells for UT and NHP cells, respectively, Figure

11G). These cells also formed polarized and lumenized acinar structures (Figure 11C). Relative to BRCA1-silenced cultures at days 10- 14, however, the total number of mitotic cells was low in the cultures of UT and NHP cells. The strong bias for planar cell divisions was lost in BRCA1-silenced cells (n=64 and n=60 mitotic cells for sh1BRCA1 and sh2BRCA1, respectively, Figure 11G,). An increase in the total number of aberrant mitoses (which were excluded from the spindle rotation analysis) in BRCA1-silenced cultures was also noted (Figure 11H).

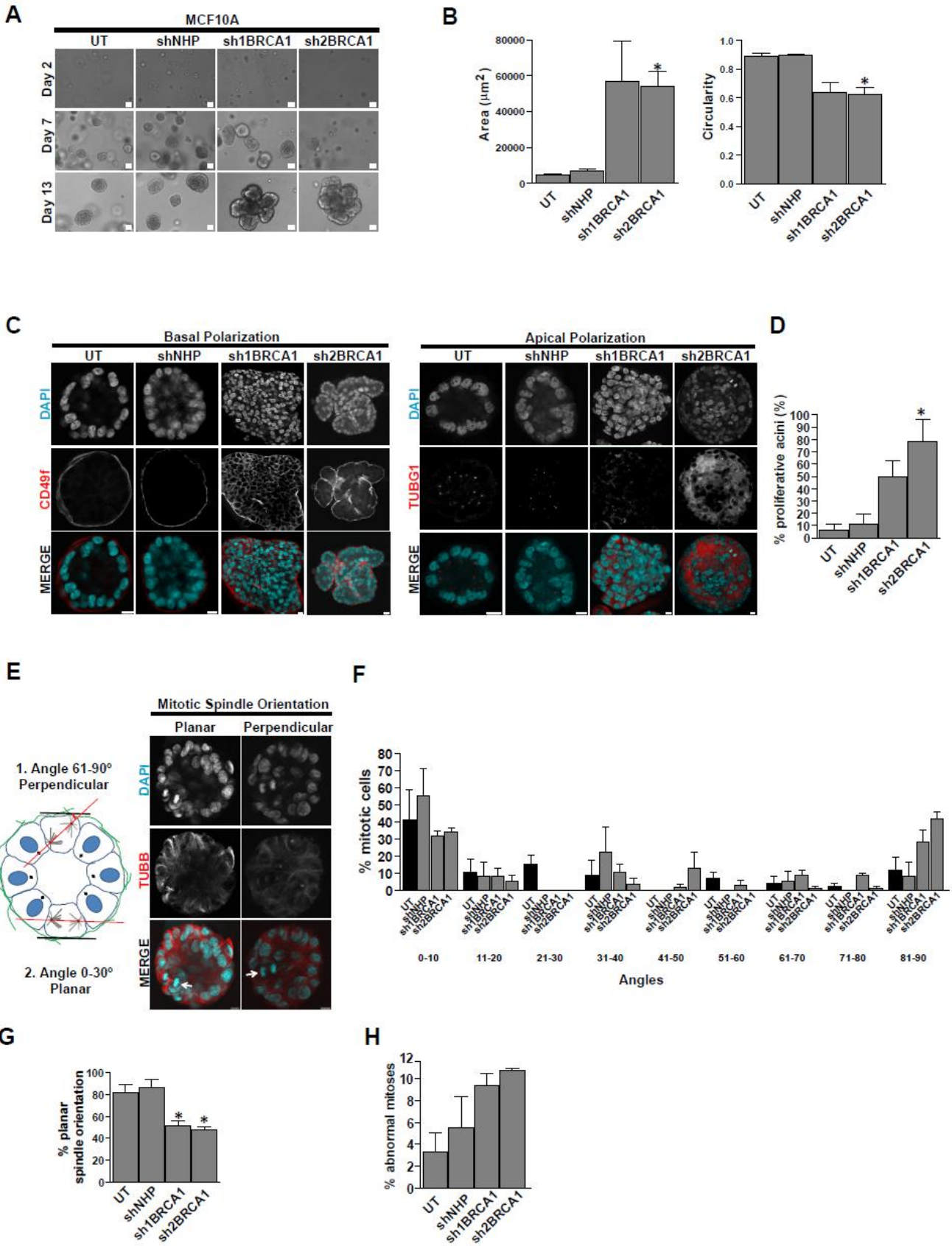
A
MCF10A
UT
shNHP
sh1BRCA1
sh2BRCA1
Day 2
Day 7
Day 13
B
Area (μm2)
Circularity
C
Basal Polarization
Apical Polarization
DAPI
CD49f
TUBG1
MERGE
D
% proliferative acini (%)
E
Mitotic Spindle Orientation
Planar
Perpendicular
1. Angle 61-90° Perpendicular
2. Angle 0-30° Planar
TUBB
F
% mitotic cells
0-10
11-20
21-30
31-40
41-50
51-60
61-70
71-80
81-90
Angles
G
% planar spindle orientation
H
% abnormal mitoses

**Figure 11. Silencing of BRCA1 disturbs acinar development, polarization and spindle orientation in 3D rBM cultures.**

**A.** MCF10A cells were untreated (UT) or infected with lentivirus encoding either a non-hairpin shRNA control (shNHP), or shRNAs targeting BRCA1 (sh1BRCA1 and sh2BRCA1. Following 48 hours post-transfection, cells were seeded at clonal density in reconstituted basement membrane (rBM). Representative images of UT, shNHP, sh1BRCA1 and sh2BRCA1 MCF10A cells, propagated in rBM for two, seven, and thirteen days are shown. N= ≥ 3 experiments. Scale bar is 10 μm.

**B.** At 48 hrs post-transduction, cells were seeded at clonal density in rBM and propagated for ten days. The size and shape of the acini is quantified in the graph. Error bars representing SEM for at least triplicate measurements. Asterisk: $p<0.05$.

**C.** At 48 hrs post-transduction, cells were seeded in rBM. At day 11, acini were fixed and stained for CD49f, TubG1 and DAPI. Representative images of acini formed from UT, shNHP, sh1BRCA1 and sh2BRCA1 treated cells are shown. Scale bars are 10 μm.

**D.** At 48 hrs post-transduction, cells were seeded in rBM. At day 11, acini were fixed and assessed for mitotic cells through the endogenous TubA1B-RFP and DAPI. Acini with one or more mitotic cells were noted as proliferative acini. The percentage of proliferative acini is quantified in the graph. Error bars representing SEM for at least triplicate measurements. Asterisk: $p<0.05$.

**E.** Cartoon demonstrating the measurement of the mitotic spindle angle in MCF10A acini. Spindle orientation relative to the basal surface of the acini was assessed in normal metaphase, anaphase, and telophase cells. Care was taken to ensure that mitotic spindle orientation was quantified in the central sections of the acini, so that parallel versus perpendicular divisions could be distinguished in 3D. Representative images of parallel and perpendicular divisions are shown. Left panel shows an anaphase cell (arrow) dividing planar (parallel) to the basal surface, while the right panel demonstrates a cell (arrow) dividing perpendicular to the basal surface of the acinus. Scale bars are 10 μm.

**F**. Mitotic spindle angles distribution for UT, shNHP, sh1BRCA1 and sh2BRCA1 treatments is shown in the graph.

**G**. At 48 hrs post-transduction, cells were seeded in rBM. Acini were fixed and mitotic spindle orientation assessed at days 9-14 in 3D culture, through the endogenous TubA1B-RFP and DAPI. The percentage of mitotic cells with planar mitotic spindle orientation in UT, shNHP, sh1BRCA1 and sh2BRCA1 treated cells is quantified in the graph. Error bars representing SEM for at least triplicate measurements. Asterisk: $p<0.05$.

**H.** Acini were fixed at days 9-14 in 3D culture, and assessed for mitotic abnormalities. The percentage of mitotic abnormalities is quantified in the graph. Error bars representing SEM for at least triplicate measurements. Asterisk: $p<0.05$.

### 3.5. Silencing of BRCA1 expression in human mammary MCF12A cells also disrupts spindle orientation.

BRCA1 may play a necessary role for correct spindle orientation but it is not clear whether its action is specific to MCF10A cells and/or ER-negative mammary cells with basal-like subtype. To explore the effect of silencing BRCA1 expression in a second non-malignant, estrogen responsive human mammary cell line that express cytokeratins 8/18, I utilized two isogenic MCF12A sublines. One of these can be induced upon addition of doxycycline to express a GFP-shRNA against BRCA1, and the other a scrambled control shRNA. Both Western blot (Figure 12A) and IF analysis (Figure 12B) of the test cells examined after 96 hours exposure to doxycycline confirmed the silencing of BRCA1. This also resulted in a significant increase in the number of mitotic cells that displayed lagging chromosomes during anaphase as well as those with post-mitotic abnormalities, including micronuclei and multinucleate cells (Figure 12C- D). A significant increase in the percentage of mitotic cells with rotated spindles was also seen in fixed cells ($p < 0.001$, 71.3 ± 14.0 mitotic cells per treatment, Figure 12E-G). These results are similar to those obtained for MCF10A cells suggesting that mammary cells may be generally dependent on BRCA1 to prevent mitotic spindle rotation, lagging chromosomes during anaphase and post-mitotic abnormalities.

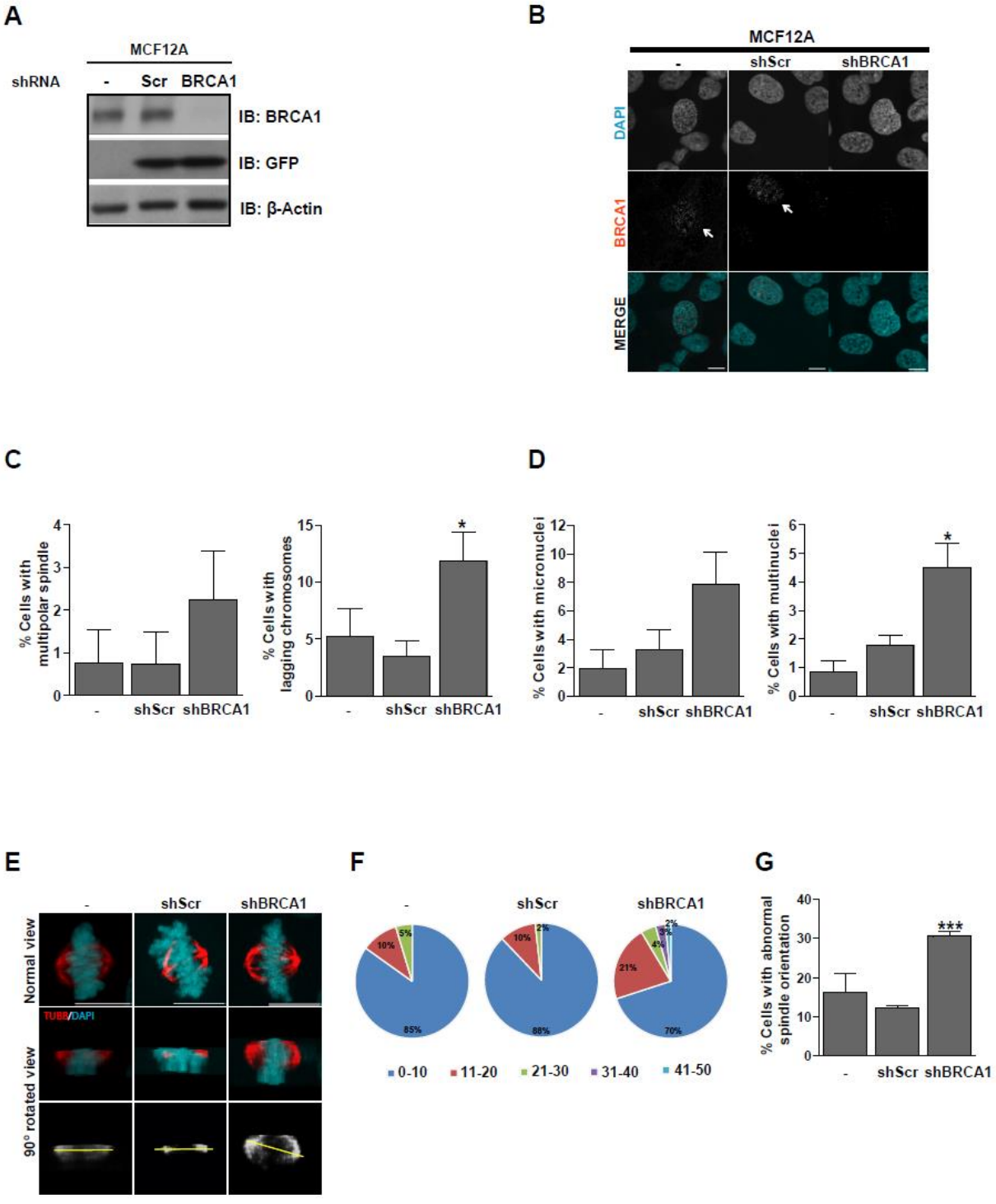
A
MCF12A
shRNA
-
Scr
BRCA1
IB: BRCA1
IB: GFP
IB: β-Actin
B
MCF12A
-
shScr
shBRCA1
DAPI
BRCA1
MERGE
C
% Cells with multipolar spindle
% Cells with lagging chromosomes
*
-
shScr
shBRCA1
D
% Cells with micronuclei
% Cells with multinuclei
*
-
shScr
shBRCA1
E
-
shScr
shBRCA1
Normal view
TUBB/DAPI
90° rotated view
F
-
shScr
shBRCA1
5%
10%
85%
2%
10%
88%
2%
3%
4%
21%
70%
0-10
11-20
21-30
31-40
41-50
G
% Cells with abnormal spindle orientation
***
-
shScr
shBRCA1

**Figure 12. BRCA1 silencing increases mitotic and post-mitotic abnormalities and alters spindle orientation.**

**A.** MCF12A cells were treated with 2 µg/ml doxycycline (dox) for 96 hrs to induce a shRNA targeting BRCA1 (shBRCA1) or scrambled shRNA control (shScr) expression relative to untreated (-) cells. Cell lysates were collected and the levels of BRCA1 and GFP were analyzed by Western blot. Actin served as a loading control.

**B.** BRCA1 localization in dox induced untreated, shScr and shBRCA1 cells, fixed with PFA and stained for BRCA1 and a nuclear counterstain DAPI at 96 hrs post-induction. Representative images of UT, shScr and shBRCA1 treated cells are shown. Scale bars are 10 µm.

**C.** Cells were fixed, stained with TubB (tubulin) and DAPI and assessed for mitotic abnormalities. The percentage of cells with multipolar spindles and lagging chromosomes is quantitated in the graphs. 150 ± 25 cells were analyzed for each group. Error bars represent SEM for triplicate measurements. Asterisk: $p<0.05$.

**D.** Fixed cells were assessed for post-mitotic abnormalities. The percentage of cells with micronuclei and multinucleate cells is quantitated in the graphs. 257 ± 36 cells were analyzed for each group. Error bars represent SEM for triplicate measurements. Asterisk: $p<0.05$.

**E.** Cells were fixed, stained with TubB and DAPI and assessed for mitotic spindle orientation relative to the growth surface. The mitotic spindle was captured by confocal microscopy through the cell body at 1 µm slices in a Z-direction. Image stacks were rotated 90° with Olympus software to allow the visualization along the growth surface. Spindle orientation was determined by measuring the angle relative to the cover glass of the line connecting the mitotic spindle poles. Scale bars are 10 µm.

**F.** Mitotic spindle angles distribution was plotted and the cut off for the normal angle positioning relative to the cover glass was determined. Angle distribution in untreated, shScr and shBRCA1 treated cells is shown in the pie charts. Three independent experimental measurements were performed for this analysis.

**G**. Normal spindle orientation was defined as 0-10° off-parallel and the percentage of cells with an abnormal spindle orientation (angle more than 10° relative to coverslip) is quantified in the bar graph. Error bars represent the SEM for triplicate measurements. 72 ± 16 cells were analyzed for each group. Asterisk: $p<0.05$.

### 3.6. Acinar morphogenesis, polarization and mitotic spindle orientation in primary human mammary epithelial cells.

Immortalized cell lines may not accurately reflect polarization and spindle rotation mechanisms operative in primary mammary epithelial cells. Accordingly, I assessed these properties in similarly cultured BCs and LPs isolated by FACS from normal adult mammary reduction mammoplasty tissue [1]. In collaboration with Dr. N Kannan (PDF in Dr. Eaves' lab at BC Cancer Research Center), these cells were seeded in rBM and then assessed for growth, polarity, and mitotic spindle orientation after 4 and 10 days of incubation. Mitotic cells were detected after 4 days in both types of cultures, but lumenization occurred between days 4 and 10 (Figure 13A). Both LP and BC-derived fractions formed spherical and lumenized structures but LP-derived acini were larger and more proliferative at day 10 (Figure 13B-C). Both fractions formed apicobasal polarized spheroids, characterized by apically-positioned centrosomes, basal deposition of CD49f, and planar mitotic divisions (Figure 13D-F). Surprisingly, the levels of abnormal mitoses, defined as either multipolar or with lagging chromosomes, was dramatically higher in LP-derived cultures (Figure 13G). These findings validate the utility of the cell line models and establish the feasibility of analyzing the effect of BRCA1 silencing in primary cells.

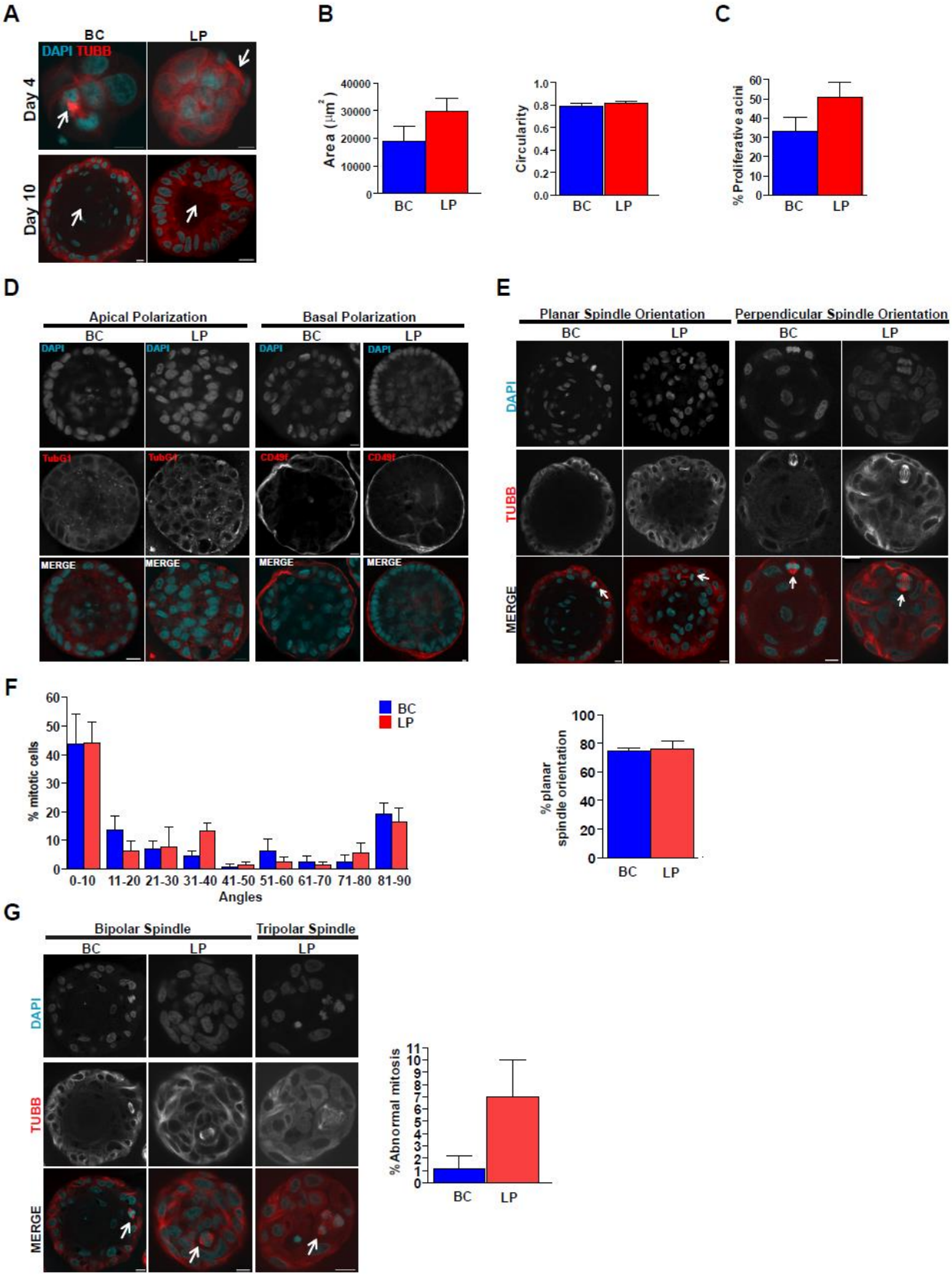
A
BC
LP
DAPI TUBB
Day 4
Day 10
B
Area (μm²)
40000
30000
20000
10000
0
BC
LP
Circularity
1.0
0.8
0.6
0.4
0.2
0.0
BC
LP
C
% Proliferative acini
60
50
40
30
20
10
0
BC
LP
D
Apical Polarization
Basal Polarization
BC
LP
DAPI
TubG1
CD49f
MERGE
E
Planar Spindle Orientation
Perpendicular Spindle Orientation
BC
LP
DAPI
TUBB
MERGE
F
% mitotic cells
BC
LP
0-10
11-20
21-30
31-40
41-50
51-60
61-70
71-80
81-90
Angles
% planar spindle orientation
100
80
60
40
20
0
BC
LP
G
Bipolar Spindle
Tripolar Spindle
BC
LP
DAPI
TUBB
MERGE
% Abnormal mitosis
11
10
9
8
7
6
5
4
3
2
1
0
BC
LP

**Figure 13. Primary mammary cells form polarized acini through directionally positioning the spindle during mitosis with minimal mitotic abnormalities in rBM.**

**A.** BC and LP cells were seeded at clonal density in reconstituted basement membrane (rBM). Acini were fixed and stained for TubB (tubulin) and a nuclear counterstain (DAPI) to delineate mitosis (arrows), lumen formation (arrows) and overall spheroid morphology at days 4 and 10 in 3D. Representative confocal images of BC and LP derived acini are shown. Scale bars are 10 μm.

**B.** BC and LP cells were propagated in matrigel for 10 days. Acini were fixed and imaged on confocal microscope. Both BC and LP derived acini were assessed for size and shape by Olympus FV10i software. The size and shape of BC and LP derived acini is quantified in the graph. 90 BC and 71 LP derived acini were assessed (n=3 experiments). Error bars representing SEM.

**C.** BC and LP cells were propagated in matrigel for 10 days. Acini were fixed and imaged on confocal microscope. Both BC and LP derived acini were assessed for proliferation by Olympus FV10i software. Acini with one or more mitotic cells were noted as proliferative acini. The percentage of proliferative acini is quantified in the graph. 403 BC and 266 LP acini assessed (at least 3 experiments). Error bars representing SEM.

**D.** BC and LP cells were propagated in matrigel for 10 days. Acini were fixed and stained for polarization markers TubG1, CD49f, and DAPI. Representative images showing polarized BC and LP derived acini. Scale bars are 10 μm.

**E.** BC and LP acini were propagated in rBM for 10 days. Acini were fixed, stained for TubB and DAPI and assessed for mitotic spindle orientation. Representative images of planar and perpendicular mitotic spindle orientation in metaphase and anaphase cells from both BC and LP fractions are shown. Mitotic spindle orientation relative to the basal surface of the acini was assessed in normal metaphase, anaphase and telophase cells. Care was taken to ensure that mitotic spindle orientation was quantified in the central sections of the acini, so that planar (mitotic spindle orientated along the plane of the basal side) versus perpendicular (spindle oriented orthogonal to the basal side) divisions could be distinguished in 3D space. The percentage of mitotic cells with planar mitotic spindle orientation in BC and LP derived acini is quantified in the graph. 73 BC and 68 LP derived acini were assessed (n=4 experiments). Error bars represent the SEM. Scale bars are 10 μm.

**F.** BC and LP acini were propagated in rBM for 10 days. Mitotic spindle angle distribution in BC and LP derived acini is quantified in the graph (n=4 experiments). Error bars represent the SEM.

**G.** BC and LP acini were propagated in rBM for 10 days. Confocal images showing normal and abnormal mitosis in BC and LP derived acini. The percentage of cells with abnormal mitosis is quantified in the graph. Total cell number assessed was 291 and 240 mitotic cells for BC and LP derived acini, respectively in four experimental measurements. Error bars represent the SEM. Scale bars are 10 μm.

## Chapter 4: Discussion and Conclusions

Loss of function mutations in *BRCA1* predispose carriers to an aggressive subtype of breast cancer that displays features characteristic of primitive mammary cells. This subtype of breast cancer is not seen in carriers of *BRCA2* mutations, which suggests the involvement of a tumour suppressor pathway distinct from the DNA damage response. At a molecular level, BRCA1 regulates the levels of the mitotic spindle protein RHAMM and BRCA1 is regulated by the mitotic kinase AURKA. Both of these gene products have recently been shown to regulate the process of mitotic spindle orientation, which is a critical pathway for the control of asymmetric division of tissue-specific stem cells. Here, I investigated the role of BRCA1 in maintaining the integrity of proliferation, polarization and mitotic spindle orientation in two immortalized human mammary cell lines, and obtained evidence of its ability to regulate mitotic spindle orientation during cell division.

### 4.1 Silencing BRCA1 augments genomic instability through control of spindle orientation in mammary cells.

In this study, I identified abnormal mitotic spindle positioning following BRCA1 depletion in mammary cells, which augmented mitotic and post-mitotic abnormalities. This perturbation of a normal mechanism to maintain genomic stability during cell division is in agreement with a well-defined role for BRCA1 [51] and with a previously reported increase in aberrant mitotic figures upon BRCA1 silencing.[49] BRCA1 has also been shown to localize with Rad51 into a functional complex involved in DNA damage repair.[131, 53] All of the above mechanisms for BRCA1 action are consistent with the observation here that silencing

BRCA1 results in an incompetent DNA damage response, an increase in the frequency of lagging chromosomes and the formation of multinucleate and micronucleted cells. Previous studies demonstrated that BRCA1 depleted mouse fibroblasts displayed defective $G_2$-M checkpoint, chromosomal aberrations, and centrosomal amplifications leading to an increase in multipolar spindle formation [132], and human breast cancer cell lines exhibited centrosomal amplifications and defective mitotic spindle assembly.[133] Upon close examination of fixed or live mammary cells following BRCA1 depletion, I did not detect an increase in multipolar spindle formation but rather alterations in spindle rotation. My findings suggests that BRCA1 is required after mitotic spindle assembly and its loss affects spindle positioning, which may be through the control of RHAMM abundance.[49] The discrepancy between my findings and those previously published might be attributed to differences in models or methodologies, including the methods and degree of BRCA1 silencing and the timing of endpoint analyses.

**4.2 Silencing of BRCA1 alters spindle rotation, but not spindle assembly duration in mammary cells.**

Mitotic spindle orientation has been shown to play a role in mouse mammary epithelia cell fate determination, proliferation and tissue homeostasis in several recent publications [93, 119, 101], but the role of mitotic spindle orientation in human mammary cells, and the players involved, has not been well established. Two opposing molecular motor complexes play a role in mitotic spindle positioning in HeLa cells: centrosomal RHAMM/CHICA complex competes with cortical NuMA/LGN complex for dynein motor protein allocation.[79] When these forces are in equilibrium, spindle alignment is established.

But when this equilibrium is disturbed, mitotic spindle tumbling increases and is detectable as mitotic spindle misorientation in fixed cells and increased spindle rotation during live imaging.[79]

A role for BRCA1 in the control of spindle rotation in human mammary cells has not been previously reported. One putative mechanism involves the control of RHAMM abundance through BRCA1-mediated post-transcriptional degradation.[49] However, BRCA1 also regulate microtubule dynamics, and the loss of BRCA1 might lead to more mobile microtubules.[134] Microtubule dynamics are important for assembly of astral microtubules, and these in turn are responsible for rotating and correctly positioning the spindle.[135] Future studies will be needed to uncover the mechanism by which BRCA1 controls spindle rotation.

It is possible that the accumulation of RHAMM, which results through depletion of BRCA1 [49], leads to defects in spindle positioning. Normally, spindles orient planar to the growth surface in mouse mammary cells [93, 119, 101], and I found a similar trend in MCF10A cells in both 2D and 3D cultures and in primary mammary BC and LP cells in 3D cultures. Interestingly, this trend was lost in BRCA1 silenced MCF-10A cells. Mitotic spindle misorientation in BRCA1 silenced cells might be implicated in the inability of these cells to polarize and growth arrest. As mitotic spindles were not positioned correctly in a dividing cell, the progeny may fail to orient appropriately in the space, which would be evident by lumen filling with daughter cells.

I did not observe major defects in mitosis duration upon BRCA1 silencing. This is in line with a published study where depletion of the tumour suppressor VHL (von Hippel-Lindau syndrome) resulted in rotated spindles with no apparent effect on mitosis duration[128]. Unlike Joukov et al. [49], I did not observe a significant increase in abnormal mitotic spindles following BRCA1 silencing in MCF10A cells. This may have a number of explanations. First, my studies were conducted in p53 competent, human mammary cells while Joukov studied *Xenopus* extracts and HeLa cells. Second, in my studies of adherent cells, I focused on the first cell divisions following BRCA1 silencing. In these first divisions, the level of multipolar spindles was low but the daughter cells were frequently aneuploid or tetraploid. Thus, it is probable that subsequent cell divisions of tetraploid cells may be multipolar due to the elevated numbers of centrosomes/ spindle poles in these cells.

During acinar morphogenesis and mammary tissue maintenance, inappropriately localized daughter cells might fail to undergo proper lineage specification.[93] Failure to compartmentalize the progeny correctly might then disturb tissue homeostasis and cell to cell communication, creating more proliferative primitive cellular fractions that are unable to growth arrest and commit to either luminal or myoepithelial lineages. Future studies are necessary to assess whether spindle rotation induced by the loss of BRCA1 alters lineage specification in human mammary progenitor fractions or in tissues from BRCA1 mutation carriers. Interestingly, the mammary stem cell hierarchy has recently been challenged, and the possible diversity of primitive mammary subsets has been described.[19, 21] Differential mitotic positioning might alter lineage specification in these primitive subsets, and needs to be investigated further along with its putative relationship to cancer.

### 4.3 Silencing BRCA1 decreases clonogenicity in adherent cultures and increases the size of structures produced in 3D assays.

BRCA1 silenced cells were unable to position the mitotic spindles correctly in the plane of division leading to post-mitotic defects. Thus, even though some of the cells were able to complete mitosis, many failed to produce functional progeny. Frequently detected post-mitotic defects during live imaging included the formation of daughter cells with micronuclei, the formation of tetraploid progeny, and cell death. BRCA1- silenced MCF10A cells also showed a decrease in clonogenicity in 2D assays. Therefore, the majority of the cells may not have been able to cope with loss of tumour suppressor BRCA1 and either growth arrested or underwent apoptosis.[35] Only cells able to survive under a low BRCA1 condition went on to produce the progeny in clonogenic assays. Notably, the cells produced exhibited genome instability with many containing micronuclei and showing aneuploidy. This is consistent with published results, showing that the loss of BRCA1 does not directly cause tumours, but enhances the genomic instability and mutation rates in other genes, thereby enhancing tumourigenesis.[132, 35]

Aberrant proliferation of MCF10A cells in 3D cultures (increase in size, decrease in circularity, and increase in proliferative/mitotic acini) was noted upon BRCA1 silencing, a phenotype consistent with previous studies.[12, 13] This observation appears in contrast with that of the decreased clonogenicity of BRCA1-silenced cells when grown in 2D cultures. However, it is likely that the silencing of BRCA1 applies a selection on cells seeded in 3D, as observed in 2D, such that those cells that form clusters may exhibit genomic instability. This selection may impede the subsequent polarization and growth arrest in 3D, which reads

out as larger, less polarized and more proliferative cellular structures at 2 weeks of culture. This is important, as the failure to growth arrest might favor transformation. Anomalies in polarization were also detected in 3D structures formed from BRCA1-silenced cells. Consistent with published studies [12, 13], BRCA1 depleted cells failed to form lumenized structures. On further examination of polarization with basal (integrins) and apical (centrosomes) markers, we found that BRCA1-silenced cells displayed defects in polarization. An inability to undergo apico-basal (luminal) polarization might dictate the type of tumours formed when BRCA1 is lost and bias for tumors that are phenotypically more similar to basal epithelia than they are to the luminal compartments.

**4.4 Implications for breast cancer treatment.**

BRCA1-tumours lack targeted therapies and tend to resist taxanes, which are common chemotherapies that prevent tubulin depolymerization.[78, 136, 134] Although BRCA1 mutated tumours are sensitive to DNA-damage inducing therapies (cisplatin) [137, 138], the side-effects on cancer-free tissues are highly detrimental. Therefore, the discovery of additional BRCA1 modes of action may enable the development of novel therapies that compensate for the loss of those actions in BRCA1-mutant breast cancers. This study delineates a mechanism of BRCA1 action that might be targeted therapeutically through the control of spindle orientation.

Aurora kinase A (AURKA) phosphorylates BRCA1 (on Ser 308) to inhibit its ubiquitinase activity.[50] AURKA has been implicated in *Drosophila* neuroblast self-renewal [139], and regulates the fate of the mouse mammary stem cells through mitotic spindle

positioning during stem cells divisions.[93] Interplay between AURKA and BRCA1 has not been explored during mitotic spindle positioning or mammary epithelial differentiation but the targeted inhibition of AURKA (through aurora kinase inhibitors, AKIs) may release the inhibitory effects of the kinase on BRCA1 function.

AKIs are readily available [140] and some are being tested for efficacy in solid tumours. In a phase II trial of MLN8237 (alisertib) for ovarian cancer resistant to platinum-based chemotherapy, it was concluded that alisertib might be effective in disease control in some patients.[141] It is possible that this could be relevant to BRCA1-mutant breast cancer, with the rationale justified in our study. AKIs might potentially be used in mammary epithelia to restore homeostasis through proliferation arrest and proper daughter cell fate determination. BRCA1 silencing had similar effects on basal, ER negative (MCF10A) and estrogen responsive (MCF12A) non malignant cell lines. This suggests that defects in spindle positioning, mitotic and post-mitotic abnormalities may not be mammary cell type-dependent, with potential broader implications for breast cancer treatment.

## Bibliography


1. Kannan, N. *et al.* Glutathione-dependent and -independent oxidative stress-control mechanisms distinguish normal human mammary epithelial cell subsets. *Proc. Natl. Acad. Sci. U. S. A.* **111,** 7789–7794 (2014).

2. Shackleton, M. *et al.* Generation of a functional mammary gland from a single stem cell. *Nature* **439,** 84–8 (2006).

3. Stingl, J. *et al.* Purification and unique properties of mammary epithelial stem cells. *Nature* **439,** 993–7 (2006).

4. Eirew, P. *et al.* A method for quantifying normal human mammary epithelial stem cells with in vivo regenerative ability. *Nat. Med.* **14,** 1384–9 (2008).

5. Eirew, P., Stingl, J. & Eaves, C. J. Quantitation of human mammary epithelial stem cells with in vivo regenerative properties using a subrenal capsule xenotransplantation assay. *Nat. Protoc.* **5,** 1945–56 (2010).

6. Stingl, J., Raouf, A., Emerman, J. T. & Eaves, C. J. Epithelial progenitors in the normal human mammary gland. *J. Mammary Gland Biol. Neoplasia* **10,** 49–59 (2005).

7. Makarem, M. *et al.* Stem Cells and the Developing Mammary Gland. *J. Mammary Gland Biol. Neoplasia* **18,** 209–219 (2013).

8. Muthuswamy, S. K. & Xue, B. Cell polarity as a regulator of cancer cell behavior plasticity. *Annu. Rev. Cell Dev. Biol.* **28,** 599–625 (2012).

9. Lim, E. *et al.* Aberrant luminal progenitors as the candidate target population for basal tumor development in BRCA1 mutation carriers. *Nat. Med.* **15,** 907–13 (2009).

10. Bissell, M. J., Rizki, A. & Mian, I. S. Tissue architecture: the ultimate regulator of breast epithelial function. *Curr. Opin. Cell Biol.* **15,** 753–762 (2003).

11. Akhtar, N. & Streuli, C. H. An integrin-ILK-microtubule network orients cell polarity and lumen formation in glandular epithelium. *Nat. Cell Biol.* **15,** 17–27 (2013).

12. Furuta, S. *et al.* Depletion of BRCA1 impairs differentiation but enhances proliferation of mammary epithelial cells. *Proc. Natl. Acad. Sci. U. S. A.* **102,** 9176–81 (2005).

13. Maxwell, C. A. *et al.* Interplay between BRCA1 and RHAMM regulates epithelial apicobasal polarization and may influence risk of breast cancer. *PLoS Biol.* **9,** 1–18 (2011).

14. Zallen, J. a. Planar polarity and tissue morphogenesis. *Cell* **129,** 1051–63 (2007).

15. Gundersen, G. G. & Worman, H. J. Nuclear positioning. *Cell* **152,** 1376–89 (2013).

16. Cicalese, A. *et al.* The tumor suppressor p53 regulates polarity of self-renewing divisions in mammary stem cells. *Cell* **138,** 1083–95 (2009).

17. Visvader, J. E. & Stingl, J. Mammary stem cells and the differentiation hierarchy: current status and perspectives. *Genes Dev.* **28,** 1143–1158 (2014).

18. Takahashi, K. & Yamanaka, S. Induction of pluripotent stem cells from mouse embryonic and adult fibroblast cultures by defined factors. *Cell* **126,** 663–76 (2006).

19. Shehata, M. *et al.* Phenotypic and functional characterisation of the luminal cell hierarchy of the mammary gland. *Breast cancer Res.* **14,** 1–19 (2012).

20. Van Keymeulen, A. *et al.* Distinct stem cells contribute to mammary gland development and maintenance. *Nature* **479,** 189–93 (2011).

21. Nguyen, L. V *et al.* Clonal analysis via barcoding reveals diverse growth and differentiation of transplanted mouse and human mammary stem cells. *Cell Stem Cell* **14,** 253–63 (2014).

22. Blanpain, C. & Fuchs, E. Plasticity of epithelial stem cells in tissue regeneration. *Science* **344,** 1242281–1–10 (2014).

23. Hughes, C. S., Postovit, L. M. & Lajoie, G. a. Matrigel: a complex protein mixture required for optimal growth of cell culture. *Proteomics* **10,** 1886–90 (2010).

24. Debnath, J., Muthuswamy, S. K. & Brugge, J. S. Morphogenesis and oncogenesis of MCF-10A mammary epithelial acini grown in three-dimensional basement membrane cultures. *Methods* **30,** 256–268 (2003).

25. Perou, C. M. *et al.* Molecular portraits of human breast tumours. *Nature* **406,** 747–52 (2000).

26. Sorlie, T. *et al.* Repeated observation of breast tumor subtypes in independent gene expression data sets. *Proc. Natl. Acad. Sci.* **100,** 8418–23 (2003).

27. Proia, T. a *et al.* Genetic predisposition directs breast cancer phenotype by dictating progenitor cell fate. *Cell Stem Cell* **8,** 149–63 (2011).

28. Lakhani SR, Jacquemier J, Sloane JP, Gusterson BA, Anderson TJ, van de Vijver MJ, Farid LM, Venter D, Antoniou A, Storfer-Isser A, Smyth E, Steel CM, Haites N, Scott RJ, Goldgar D, Neuhausen S, Daly PA, Ormiston W, McManus R, Scherneck S, Ponder BA, Ford D, Peto J, Stoppa-Lyonnet D, Bignon YJ, Struewing JP, Spurr NK, Bishop DT, Klijn JG, Devilee P, Cornelisse CJ, Lasset C, Lenoir G, Barkardottir RB, Egilsson V, Hamann U, Chang-Claude J, Sobol H, Weber B, Stratton MR, Easton DF. Multifactorial analysis of differences between sporadic breast cancers and cancers involving BRCA1 and BRCA2 mutations. *J. Natl. Cancer Inst.* **90,** 1138–1145 (1998).

29. Palacios, J. *et al.* Immunohistochemical Characteristics Defined by Tissue Microarray of Hereditary Breast Cancer Not Attributable to BRCA1 or BRCA2 Mutations : Differences from Breast Carcinomas Arising in BRCA1 and BRCA2 Mutation Carriers. *Clin. Cancer Res.* **9,** 3606–3614 (2003).

30. Honrado, E., Benítez, J. & Palacios, J. The molecular pathology of hereditary breast cancer: genetic testing and therapeutic implications. *Mod. Pathol.* **18,** 1305–20 (2005).

31. Prat, A. & Perou, C. M. Deconstructing the molecular portraits of breast cancer. *Mol. Oncol.* **5,** 5–23 (2011).

32. Slamon, D. J. *et al.* Studies of the HER-2/neu proto-oncogene in human breast and ovarian cancer. *Science* **244,** 707–12 (1989).

33. Foulkes, Smith, R.-F. Triple-Negative Breast Cancer. *N. Engl. J. Med.* **363,** 1938–1948 (2010).

34. Cheang, M. C. U. *et al.* Basal-like breast cancer defined by five biomarkers has superior prognostic value than triple-negative phenotype. *Clin. cancer Res.* **14,** 1368–76 (2008).

35. Deng, C.-X. BRCA1: cell cycle checkpoint, genetic instability, DNA damage response and cancer evolution. *Nucleic Acids Res.* **34,** 1416–26 (2006).

36. Campeau, P. M., Foulkes, W. D. & Tischkowitz, M. D. Hereditary breast cancer: new genetic developments, new therapeutic avenues. *Hum. Genet.* **124,** 31–42 (2008).

37. Lee, J.-H. & Paull, T. T. Activation and regulation of ATM kinase activity in response to DNA double-strand breaks. *Oncogene* **26,** 7741–8 (2007).

38. Pujana, M. A. *et al.* Network modeling links breast cancer susceptibility and centrosome dysfunction. *Nat. Genet.* **39,** 1338–49 (2007).

39. Levy-Lahad, E. Fanconi anemia and breast cancer susceptibility meet again. *Nat. Genet.* **39,** 142–143 (2007).

40. Cantor, S. B. & Andreassen, P. R. Assessing the Link Between BACH1 and BRCA1 in the FA Pathway. *Cell Cycle* **5,** 164–167 (2006).

41. Shuhei Matsuoka, Mingxia Huang, S. J. E. Linkage of ATM to Cell Cycle Regulation by the Chk2 Protein Kinase. *Science* **282,** 1893–1897 (1998).

42. Meijers-Heijboer, H. *et al.* Low-penetrance susceptibility to breast cancer due to CHEK2(*)1100delC in noncarriers of BRCA1 or BRCA2 mutations. *Nat. Genet.* **31,** 55–9 (2002).

43. Venkitaraman, A. R. Functions of BRCA1 and BRCA2 in the biological response to DNA damage. *J. Cell Sci.* **114,** 3591–3598 (2001).

44. Miki, Y. *et al.* A Strong Candidate for the Breast and Ovarian Cancer Susceptibility Gene BRCA1. *Science* **266,** 66–71 (1994).

45. Stephens, P. J. *et al.* The landscape of cancer genes and mutational processes in breast cancer. *Nature* **486,** 400–4 (2012).

46. Nathanson, K. L. *et al.* CGH-targeted linkage analysis reveals a possible BRCA1 modifier locus on chromosome 5q. *Hum. Mol. Genet.* **11,** 1327–32 (2002).

47. Waddell, N. *et al.* Subtypes of familial breast tumours revealed by expression and copy number profiling. *Breast Cancer Res. Treat.* **123,** 661–77 (2010).

48. Curtis, C., Shah, S. P., Chin, S. & Turashvili, G. The genomic and transcriptomic architecture of 2 , 000 breast tumours reveals novel subgroups. *Nature* **486,** 346–352 (2012).

49. Joukov, V. *et al.* The BRCA1/BARD1 heterodimer modulates ran-dependent mitotic spindle assembly. *Cell* **127,** 539–52 (2006).

50. Sankaran, S., Crone, D. E., Palazzo, R. E. & Parvin, J. D. Aurora-A Kinase Regulates Breast Cancer − Associated Gene 1 Inhibition of Centrosome-Dependent Microtubule Nucleation. *J. Cancer Res.* **67,** 11186–11194 (2007).

51. Venkitaraman, A. R. Cancer suppression by the chromosome custodians, BRCA1 and BRCA2. *Science* **343,** 1470–5 (2014).

52. Roy, R., Chun, J. & Powell, S. N. BRCA1 and BRCA2: different roles in a common pathway of genome protection. *Nat. Rev. Cancer* **12,** 68–78 (2012).

53. Cousineau, I., Abaji, C. & Belmaaza, A. BRCA1 regulates RAD51 function in response to DNA damage and suppresses spontaneous sister chromatid replication slippage: implications for sister chromatid cohesion, genome stability, and carcinogenesis. *Cancer Res.* **65,** 11384–91 (2005).

54. Pathania, S. *et al.* BRCA1 Is Required for Postreplication Repair after UV-Induced DNA Damage. *Mol. Cell* **44,** 235–251 (2011).

55. Davies, a a *et al.* Role of BRCA2 in control of the RAD51 recombination and DNA repair protein. *Mol. Cell* **7,** 273–82 (2001).

56. Rosen, E. M. & Pishvaian, M. J. Targeting the BRCA1/2 tumor suppressors. *Curr. Drug Targets* **15,** 17–31 (2014).

57. Turner, N., Tutt, A. & Ashworth, A. Hallmarks of "BRCAness" in sporadic cancers. *Nat. Rev.* **4,** 1–6 (2004).

58. Parmigiani, S. C. and G. Meta-Analysis of BRCA1 and BRCA2 Penetrance. *J. Clin. Oncol.* **25,** 1329–1333 (2007).

59. Bogdanova, N. V *et al.* High frequency and allele-specific differences of BRCA1 founder mutations in breast cancer and ovarian cancer patients from Belarus. *Clin. Genet.* **78,** 364–72 (2010).

60. Futreal, P. a *et al.* BRCA1 mutations in primary breast and ovarian carcinomas. *Science* **266,** 120–2 (1994).

61. Clark, S. L., Rodriguez, A. M., Snyder, R. R., Hankins, G. D. V & Boehning, D. Structure-Function Of The Tumor Suppressor BRCA1. *Comput. Struct. Biotechnol. J.* **1,** 1–8 (2012).

62. Wu LC, Wang ZW, Tsan JT, Spillman MA, Phung A, Xu XL, Yang MC, Hwang LY, Bowcock AM, B. R. Identification of a RING protein that can interact in vivo with the BRCA1 gene product. *Nat. Genet.* **14,** 430–440 (1996).

63. Baer, R. & Ludwig, T. The BRCA1/BARD1 heterodimer, a tumor suppressor complex with ubiquitin E3 ligase activity. *Curr. Opin. Genet. Dev.* **12,** 86–91 (2002).

64. Ouchi, M. *et al.* BRCA1 Phosphorylation by Aurora-A in the Regulation of G 2 to M Transition. *Oncotarget* **279,** 19643–19648 (2004).

65. Mccarthy, E. E., Celebi, J. T., Baer, R. & Ludwig, T. Loss of Bard1 , the Heterodimeric Partner of the Brca1 Tumor Suppressor , Results in Early Embryonic Lethality and Chromosomal Instability. *Mol. Cell. Biol.* **23,** 5056–5063 (2003).

66. Shakya, R. *et al.* The basal-like mammary carcinomas induced by Brca1 or Bard1 inactivation implicate the BRCA1/BARD1 heterodimer in tumor suppression. *Proc. Natl. Acad. Sci.* **105,** 7040–5 (2008).

67. Shakya, R. *et al.* BRCA1 tumor suppression depends on BRCT phosphoprotein binding, but not its E3 ligase activity. *Science* **334,** 525–8 (2011).

68. Reid, L. J. *et al.* E3 ligase activity of BRCA1 is not essential for mammalian cell viability or homology-directed repair of double-strand DNA breaks. *Proc. Natl. Acad. Sci.* **105,** 20876–81 (2008).

69. Molyneux, G. *et al.* BRCA1 basal-like breast cancers originate from luminal epithelial progenitors and not from basal stem cells. *Cell Stem Cell* **7,** 403–17 (2010).

70. Livasy, C. a *et al.* Phenotypic evaluation of the basal-like subtype of invasive breast carcinoma. *Mod. Pathol.* **19,** 264–71 (2006).

71. Foulkes, W. D. BRCA1 functions as a breast stem cell regulator. *J. Med. Genet.* **41,** 1–5 (2004).

72. Neve, R. M. *et al.* A collection of breast cancer cell lines for the study of functionally distinct cancer subtypes. *Cancer Cell* **10,** 515–527 (2006).

73. Marshall, A. M., Pai, V. P., Sartor, M. a & Horseman, N. D. In vitro multipotent differentiation and barrier function of a human mammary epithelium. *Cell Tissue Res.* **335,** 383–95 (2009).

74. Sarrió, D. *et al.* Epithelial-mesenchymal transition in breast cancer relates to the basal-like phenotype. *Cancer Res.* **68,** 989–97 (2008).

75. Liu, S. *et al.* BRCA1 regulates human mammary stem/progenitor cell fate. *Proc. Natl. Acad. Sci.* **105,** 1680–5 (2008).

76. Visvader, J. E. Keeping abreast of the mammary epithelial hierarchy and breast tumorigenesis. *Genes Dev.* **23,** 2563–77 (2009).

77. Walczak, C. E., Cai, S. & Khodjakov, A. Mechanisms of chromosome behaviour during mitosis. *Nat. Rev. Mol. Cell Biol.* **11,** 91–102 (2010).

78. Janssen, a & Medema, R. H. Mitosis as an anti-cancer target. *Oncogene* **30,** 2799–809 (2011).

79. Dunsch, A. K. *et al.* Dynein light chain 1 and a spindle-associated adaptor promote dynein asymmetry and spindle orientation. *J. Cell Biol.* 1–16 (2012). doi:10.1083/jcb.201202112

80. Itzkovitz, S., Blat, I. C., Jacks, T., Clevers, H. & van Oudenaarden, A. Optimality in the development of intestinal crypts. *Cell* **148,** 608–19 (2012).

81. Knoblich, J. a. Asymmetric cell division: recent developments and their implications for tumour biology. *Nat. Rev. Mol. Cell Biol.* **11,** 849–60 (2010).

82. Chang, J. T. *et al.* Asymmetric T lymphocyte division in the initiation of adaptive immune responses. *Science* **315,** 1687–91 (2007).

83. Oliaro, J. *et al.* Asymmetric cell division of T cells upon antigen presentation uses multiple conserved mechanisms. *J. Immunol.* **185,** 367–75 (2010).

84. Devenport, D. & Fuchs, E. Planar polarization in embryonic epidermis orchestrates global asymmetric morphogenesis of hair follicles. *Nat. Cell Biol.* **10,** 1257–68 (2008).

85. Quyn, A. J. *et al.* Spindle orientation bias in gut epithelial stem cell compartments is lost in precancerous tissue. *Cell Stem Cell* **6,** 175–81 (2010).

86. Falconer, E. *et al.* Identification of sister chromatids by DNA template strand sequences. *Nature* **463,** 93–7 (2010).

87. Barker, N. *et al.* Identification of stem cells in small intestine and colon by marker gene Lgr5. *Nature* **449,** 1003–7 (2007).

88. Korinek, V. *et al.* Depletion of epithelial stem-cell compartments in the small intestine of mice lacking Tcf-4. *Nat. Genet.* **19,** 379–83 (1998).

89. Sato, T. *et al.* Paneth cells constitute the niche for Lgr5 stem cells in intestinal crypts. *Nature* **469,** 415–8 (2011).

90. Inaba, M. & Yamashita, Y. M. Asymmetric stem cell division: precision for robustness. *Cell Stem Cell* **11,** 461–9 (2012).

91. Siller, K. H., Cabernard, C. & Doe, C. Q. The NuMA-related Mud protein binds Pins and regulates spindle orientation in Drosophila neuroblasts. *Nat. Cell Biol.* **8,** 594–600 (2006).

92. Troy, A. *et al.* Coordination of satellite cell activation and self-renewal by Par-complex-dependent asymmetric activation of p38α/β MAPK. *Cell Stem Cell* **11,** 541–53 (2012).

93. Regan, J. L. *et al.* Aurora A Kinase Regulates Mammary Epithelial Cell Fate by Determining Mitotic Spindle Orientation in a Notch-Dependent Manner. *Cell Rep.* **4,** 110–123 (2013).

94. Noatynska, A., Gotta, M. & Meraldi, P. Mitotic spindle (DIS)orientation and DISease: cause or consequence? *J. Cell Biol.* **199,** 1025–35 (2012).

95. Hutterer, A. *et al.* Mitotic activation of the kinase Aurora-A requires its binding partner Bora. *Dev. Cell* **11,** 147–57 (2006).

96. Cayouette, M. & Raff, M. Asymmetric segregation of Numb: a mechanism for neural specification from Drosophila to mammals. *Nat. Neurosci.* **5,** 1265–9 (2002).

97. Seki, A., Coppinger, J. a, Jang, C.-Y., Yates, J. R. & Fang, G. Bora and the kinase Aurora a cooperatively activate the kinase Plk1 and control mitotic entry. *Science* **320,** 1655–8 (2008).

98. Macůrek, L. *et al.* Polo-like kinase-1 is activated by aurora A to promote checkpoint recovery. *Nature* **455,** 119–23 (2008).

99. Luca, M. De, Lavia, P. & Guarguaglini, G. a functional interplay between aurora-A, Plk1 and TPX2 at spindle poles. *cell cycle* **5,** 296–303 (2006).

100. Chan, E. H. Y., Santamaria, A., Silljé, H. H. W. & Nigg, E. a. Plk1 regulates mitotic Aurora A function through betaTrCP-dependent degradation of hBora. *Chromosoma* **117,** 457–69 (2008).

101. Villegas, E. *et al.* Plk2 regulates mitotic spindle orientation and mammary gland development. *Development* **141,** 1562–1571 (2014).

102. Vale, R. D. The Molecular Motor Toolbox for Intracellular Transport. *Cell* **112,** 467–480 (2003).

103. Pavin, N. & Tolić-Nørrelykke, I. M. Dynein, microtubule and cargo: a ménage à trois. *Biochem. Soc. Trans.* **41,** 1731–5 (2013).

104. Varma, D., Monzo, P., Stehman, S. a & Vallee, R. B. Direct role of dynein motor in stable kinetochore-microtubule attachment, orientation, and alignment. *J. Cell Biol.* **182,** 1045–54 (2008).

105. Wojcik, E. *et al.* Kinetochore dynein: its dynamics and role in the transport of the Rough deal checkpoint protein. *Nat. Cell Biol.* **3,** 1001–7 (2001).

106. Kotak, S., Busso, C. & Gönczy, P. Cortical dynein is critical for proper spindle positioning in human cells. *J. Cell Biol.* **199,** 97–110 (2012).

107. Kiyomitsu, T. & Cheeseman, I. M. Cortical dynein and asymmetric membrane elongation coordinately position the spindle in anaphase. *Cell* **154,** 391–402 (2013).

108. Kiyomitsu, T. & Cheeseman, I. M. Chromosome- and spindle-pole-derived signals generate an intrinsic code for spindle position and orientation. *Nat. Cell Biol.* **14,** 311–7 (2012).

109. Kotak, S., Busso, C. & Gönczy, P. NuMA interacts with phosphoinositides and links the mitotic spindle with the plasma membrane. *EMBO J.* 1–16 (2014). doi:10.15252/embj.201488147

110. Zheng, Z. *et al.* LGN regulates mitotic spindle orientation during epithelial morphogenesis. *J. Cell Biol.* **189,** 275–88 (2010).

111. Peyre, E. *et al.* A lateral belt of cortical LGN and NuMA guides mitotic spindle movements and planar division in neuroepithelial cells. *J. Cell Biol.* **193,** 141–54 (2011).

112. Maxwell, C. A. *et al.* RHAMM Is a Centrosomal Protein That Interacts with Dynein and Maintains Spindle Pole Stability. *Mol. Biol. Cell* **14,** 2262–2276 (2003).

113. Chen H, Mohan P, Jiang J, Nemirovsky O, He D, Fleisch MC, Niederacher D, Pilarski LM, Lim CJ, M. C. Spatial regulation of Aurora A activity during mitotic spindle assembly requires RHAMM to correctly localize TPX2. *Cell Cycle* **13,** 2248–2261 (2014).

114. Maxwell, C. A., Keats, J. J., Belch, A. R., Pilarski, L. M. & Reiman, T. Receptor for Hyaluronan-Mediated Motility Correlates with Centrosome Abnormalities in Multiple Myeloma and Maintains Mitotic Integrity. *Cancer Res* **65,** 850–860 (2005).

115. Santamaria, A. *et al.* The Plk1-dependent phosphoproteome of the early mitotic spindle. *Mol. Cell. proteomics* **10,** 1–18 (2011).

116. Jiang, J., Mohan, P. & Maxwell, C. a. The cytoskeletal protein RHAMM and ERK1/2 activity maintain the pluripotency of murine embryonic stem cells. *PLoS One* **8,** 1–12 (2013).

117. Choudhary, M. *et al.* Putative role of hyaluronan and its related genes, HAS2 and RHAMM, in human early preimplantation embryogenesis and embryonic stem cell characterization. *Stem Cells* **25,** 3045–57 (2007).

118. Ferguson, D. J. P. An ultrastructural study of mitosis and cytokinesis in normal "resting" human breast. *Cell Tissue Res.* **252,** 581–587 (1988).

119. Elias, S. *et al.* Huntingtin regulates mammary stem cell division and differentiation. *Stem cell reports* **2,** 491–506 (2014).

120. Godin, J. D. *et al.* Huntingtin is required for mitotic spindle orientation and mammalian neurogenesis. *Neuron* **67,** 392–406 (2010).

121. Kannan, N. *et al.* The Luminal Progenitor Compartment of the Normal Human Mammary Gland Constitutes a Unique Site of Telomere Dysfunction. *Stem Cell Reports* **1,** 28–37 (2013).

122. Yui, S. *et al.* Functional engraftment of colon epithelium expanded in vitro from a single adult Lgr5+ stem cell. *Nat. Med.* **18,** 618–623 (2012).

123. Sato, T. *et al.* Single Lgr5 stem cells build crypt-villus structures in vitro without a mesenchymal niche. *Nature* **459,** 262–5 (2009).

124. Koo, B.-K. *et al.* Controlled gene expression in primary Lgr5 organoid cultures. *Nat. Methods* **9,** 81–3 (2012).

125. Mohan, P. *et al.* Genomic imbalance of HMMR / RHAMM regulates the sensitivity and response of malignant peripheral nerve sheath tumour cells to aurora kinase inhibition. *Oncotarget* **4,** 80–93 (2013).

126. Musacchio, A. & Salmon, E. D. The spindle-assembly checkpoint in space and time. *Nat. Rev. Mol. Cell Biol.* **8,** 379–93 (2007).

127. Lampson, M. A. & Cheeseman, I. M. Sensing centromere tension: Aurora B and the regulation of kinetochore function. *trends cell biol* **21,** 133–140 (2011).

128. Thoma, C. R. *et al.* VHL loss causes spindle misorientation and chromosome instability. *Nat. Cell Biol.* **11,** 994–1001 (2009).

129. Wang, R.-H., Yu, H. & Deng, C.-X. A requirement for breast-cancer-associated gene 1 (BRCA1) in the spindle checkpoint. *Proc. Natl. Acad. Sci.* **101,** 17108–13 (2004).

130. Cerruti, B. *et al.* Polarity, cell division, and out-of-equilibrium dynamics control the growth of epithelial structures. *J. Cell Biol.* **203,** 359–72 (2013).

131. Scully, R. *et al.* Association of BRCA1 with Rad51 in mitotic and meiotic cells. *Cell* **88,** 265–75 (1997).

132. Xu, X. *et al.* Conditional mutation of Brca1 in mammary epithelial cells results in blunted ductal morphogenesis and tumour formation. *Nat. Genet.* **22,** 37–43 (1999).

133. Brodie, K. M. & Henderson, B. R. Characterization of BRCA1 centrosome targeting, dynamics and function: A role for the nuclear export signal, CRM1 and Aurora A kinase. *J. Biol. Chem.* **1,** 1–17 (2012).

134. M Sung and P Giannakakou. BRCA1 regulates microtubule dynamics and taxane-induced apoptotic cell signaling. *Oncogene* **33,** 1418–1428 (2014).

135. Pease, J. C. & Tirnauer, J. S. Mitotic spindle misorientation in cancer--out of alignment and into the fire. *J. Cell Sci.* **124,** 1007–16 (2011).

136. Byrski, T. *et al.* Response to neo-adjuvant chemotherapy in women with BRCA1-positive breast cancers. *Breast Cancer Res. Treat.* **108,** 289–96 (2008).

137. Zhang, J. & Powell, S. N. The role of the BRCA1 tumor suppressor in DNA double-strand break repair. *Mol. Cancer Res.* **3,** 531–9 (2005).

138. Bhattacharyya, a, Ear, U. S., Koller, B. H., Weichselbaum, R. R. & Bishop, D. K. The breast cancer susceptibility gene BRCA1 is required for subnuclear assembly of Rad51 and survival following treatment with the DNA cross-linking agent cisplatin. *J. Biol. Chem.* **275,** 23899–903 (2000).

139. Lee, C.-Y. *et al.* Drosophila Aurora-A kinase inhibits neuroblast self-renewal by regulating aPKC/Numb cortical polarity and spindle orientation. *Genes Dev.* **20,** 3464–74 (2006).

140. Kollareddy, M. *et al.* Aurora kinase inhibitors: progress towards the clinic. *Invest. New Drugs* **30,** 2411–32 (2012).

141. Matulonis, U. a *et al.* Phase II Study of MLN8237 (alisertib), An Investigational Aurora A Kinase Inhibitor, In Patients With Platinum-Resistant Or -Refractory Epithelial Ovarian, Fallopian Tube, Or Primary Peritoneal Carcinoma. *Gynecol. Oncol.* **8237,** 1–7 (2012).